ProxiFit: Proximity Magnetic Sensing Using a Single Commodity Mobile toward Holistic Weight Exercise Monitoring

JIHA KIM, POSTECH, South Korea
YOUNHO NAM, POSTECH, South Korea
JUNGEUN LEE, POSTECH, South Korea
YOUNG-JOO SUH*, POSTECH, South Korea
INSEOK HWANG*, POSTECH, South Korea

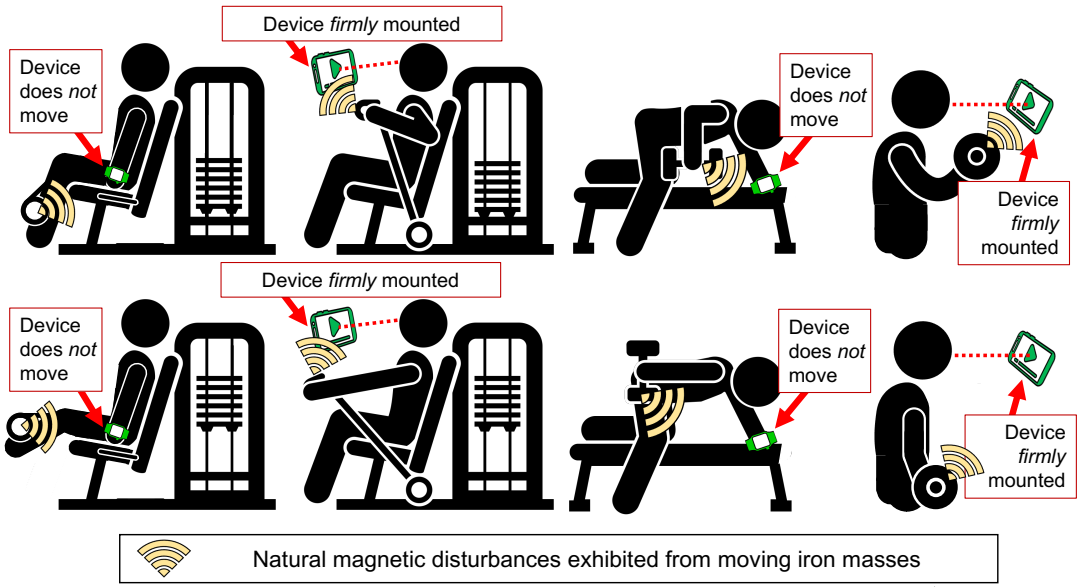

Fig. 1. ProxiFit introduces proximity magnetic sensing for holistic weight exercise tracking with only a single commodity personal device, in two possible configurations: (1) with a single wearable (wrist-worn naturally), or (2) with a single smartphone (mounted for convenient viewing).

*Co-corresponding authors.

Authors' addresses: Jiha Kim, jiha.kim@postech.ac.kr, POSTECH, Cheongam-ro 77, Pohang, Gyeongbuk, South Korea, 37673; Younho Nam, younho@postech.ac.kr, POSTECH, Cheongam-ro 77, Pohang, Gyeongbuk, South Korea, 37673; Jungeun Lee, jelee@postech.ac.kr, POSTECH, Cheongam-ro 77, Pohang, Gyeongbuk, South Korea, 37673; Young-Joo Suh, yjsuh@postech.ac.kr, POSTECH, Cheongam-ro 77, Pohang, Gyeongbuk, South Korea, 37673; Inseok Hwang, i.hwang@postech.ac.kr, POSTECH, Cheongam-ro 77, Pohang, Gyeongbuk, South Korea, 37673.

2474-9567/2023/9-ART105 $15.00
https://doi.org/10.1145/3610920

Although many works bring exercise monitoring to smartphone and smartwatch, inertial sensors used in such systems require device to be in motion to detect exercises. We introduce ProxiFit, a highly practical on-device exercise monitoring system capable of classifying and counting exercises even if the device stays still. Utilizing novel proximity sensing of natural magnetism in exercise equipment, ProxiFit brings (1) a new category of exercise not involving device motion such as lower-body machine exercise, and (2) a new off-body exercise monitoring mode where a smartphone can be conveniently viewed in front of the user during workouts. ProxiFit addresses common issues of faint magnetic sensing by choosing appropriate preprocessing, negating adversarial motion artifacts, and designing a lightweight yet noise-tolerant classifier. Also, application-specific challenges such as a wide variety of equipment and the impracticality of obtaining large datasets are overcome by devising a unique yet challenging training policy. We evaluate ProxiFit on up to 10 weight machines (5 lower- and 5 upper-body) and 4 free-weight exercises, on both wearable and signage mode, with 19 users, at 3 gyms, over 14 months, and verify robustness against user and weather variations, spatial and rotational device location deviations, and neighboring machine interference.

CCS Concepts: • **Human-centered computing → Ubiquitous computing**; *Interactive systems and tools*; • **Hardware → Sensor applications and deployments**.

Additional Key Words and Phrases: exercise monitoring, magnetic sensing, wearable, proximity sensing

ACM Reference Format:
Jiha Kim, Younho Nam, Jungeun Lee, Young-Joo Suh, and Inseok Hwang. 2023. ProxiFit: Proximity Magnetic Sensing Using a Single Commodity Mobile toward Holistic Weight Exercise Monitoring. *Proc. ACM Interact. Mob. Wearable Ubiquitous Technol.* 7, 3, Article 105 (September 2023), 32 pages. https://doi.org/10.1145/3610920

1 INTRODUCTION

With the proliferation of commodity mobiles and wearables, many gym-goers use their devices at gyms for exercise tracking [1, 2, 6, 7, 22]. Prior researches report that manual logging of health data is burdensome [21] and thus pervasive fitness tracking should be adopted [116], and gym-goers' preference are in line with the claim [22, 120, 125]. Extensive efforts have been put into the pervasive tracking of gym exercises. While approaches with external instrumentation [47, 72, 114] or custom-built wearables [29, 98, 132] are capable of omniscient tracking, approaches with personal commodity mobile/wearable such as smartphones or watches have unique merits: zero hardware investment, gym-independent applicability, and keeping gym-goers' privacy from third-party. Commercial apps and research prototypes with smartphones, watches, or other wearables have been developed. Each work covers a certain subset of gym exercises, to which they offer tracking features such as exercise classification and repetition counting [16, 120].

Despite the variety, exercise tracking systems with a commodity personal device mainly rely on a common principle: having inertial measurement units (IMU) – accelerometer and gyroscope – sense the motion of the exercising body part on which the device is worn. In the real world, this principle poses inherent constraints such that exercises not moving the body part on which the device is worn cannot be tracked. Each gym exercise engages specific body parts moving, which may or may not include where the device is worn. Figure 2(a) and (b) illustrate example exercises that a smartwatch, worn on the left wrist, can and cannot track, respectively. For brevity, this paper uses '$\mathcal{M}$-*Exercise*' to denote an exercise where the device $\mathcal{M}$-oves along with the exercising limbs, and '$\mathcal{S}$-*Exercise*' to denote an exercise where the device stays $\mathcal{S}$-tationary during exercise. Unless stated otherwise, we assume the device is a smartwatch worn on the left wrist, i.e., likely the most-sold wearable worn in the most frequent way. Figure 3 and 4 illustrate the major exercises seen in most gyms, categorized into $\mathcal{S}$-*Exercise* and $\mathcal{M}$-*Exercise*, respectively. Note each exercise's acronym (e.g., LP for leg press, BT for butterfly, etc.) in the figures, as they are frequently referred to in the paper.

Our surveys on three local gyms reveal 22 of 60 machines are of $\mathcal{S}$-*Exercise*, which means 37% of machines in those gyms (plus free-weight exercises, e.g., dumbbells, on a non-device arm) cannot be supported by conventional IMU-based systems. Typical approaches try to mitigate the coverage limitation by introducing more sensors to

different body parts [32, 103, 122, 125, 131] or relocate the device to the exercising body part on-demand [73]. However, such approaches pose practicality concerns as they force the users to frequently change the device position or buy extra devices.

Another problem is that the concept of inertial sensing diminishes the usability of smartphones – i.e., the most commodity personal device. The display, a highly advertised feature of modern smartphones, is often integral in natural user experiences. Direct visibility of the smartphone's display during workouts can deliver favorable user experiences (UX), e.g., watching guidance videos or enjoying entertainment content. Numerous guidance videos, including some produced by exercise equipment manufacturers [46, 51], are created to assist users in performing effective and safe workouts by helping them maintain correct posture during exercise. Research also reports that entertainment consumption during workouts can exert a positive psychological impact, or can be useful as a distraction redirecting attention from difficult demanding exercises [24]. While some exercise machines come equipped with built-in screens [18], most of them do not, necessitating the separate mounting of smartphones to the machine to accommodate such visual interaction needs during workouts. Products such as *Belkin Fitness Mount* [10] allow users to conveniently attach their smartphones to gym equipment, and are well received in the market where 644 ratings average to 4.4 of 5 stars. Unfortunately, an armband–a common practice to make a phone move along exercises, renders the display not in the line-of-sight, taking away its main interface. Not to mention that $\mathcal{S}$-*Exercise* is still out of coverage.

In this light, we identify that the following problem is yet to be explored, despite its strong practical merit:

Problem Statement

To develop a weight-exercise tracking system, that satisfies *all* of the following conditions in favor of practicality:

(1) supports a **holistic coverage** of weight machines and free-weight exercises, even if the device is not in motion along with the exercise, and
(2) requires only a **single**, **commodity**, **commercial off-the-shelf (COTS)** device that most people own, and
(3) preserves the **natural way** of using that device, i.e., a watch stays worn on the wrist, a smartphone display stays in the line-of-sight, and
(4) assumes **no external instrumentation**, e.g., environment or equipment, to get the system to work.

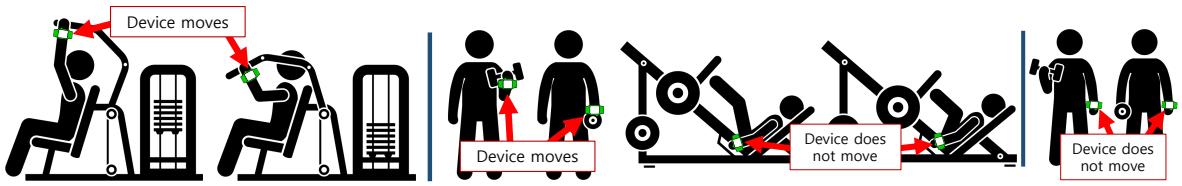

(a) Exercises involving device motion ($\mathcal{M}$-*Exercise*) (e.g., Shoulder Press (SP) & Biceps Curl (BC) on left arm)

(b) Exercises *not* involving device motion ($\mathcal{S}$-*Exercise*) (e.g., Leg Press (LP) & Biceps Curl (BC) on right arm)

Fig. 2. An example of different dynamics in two categories of exercise – $\mathcal{M}$-*Exercise* and $\mathcal{S}$-*Exercise*, assuming a left-wrist-worn smartwatch. Notice the yellow smartwatch moves along with the exercise or stays still depending on exercise categories.

We propose ProxiFit[1], an end-to-end weight exercise tracking system that leverages *magnetic field sensing in proximity to gym equipment*. Our intuition is that most gym equipment is largely made of ferrous metal – iron or steel, in the machine structure, weight stack, and free-weight equipment such as dumbbells and barbells. Unlike conventional IMU approaches, our magnetic approach eliminates the necessity of the device moving along the exercise motions. A moving mass of ferrous metal disturbs the magnetic field in its vicinity, which is sensible by a nearby magnetometer that may stay still. This principle enables ProxiFit to support the entire family of $\mathcal{S}$*-Exercise*, and thereby **satisfy condition (1)** in the problem statement. Note that supporting $\mathcal{M}$*-Exercise* is straightforward; later we demonstrate two implementations – to co-exist with a conventional IMU pipeline or to directly apply magnetic sensing to $\mathcal{M}$*-Exercise* as well.

ProxiFit runs on a single commodity personal device, i.e., *either (not both)* a smartwatch or a smartphone, using only its built-in magnetometer, IMUs, and local processing, thereby making ProxiFit **satisfy condition (2)** in the problem statement. Figure 3 and 5 depict the two usage modes of ProxiFit. The ***wearable mode*** (primarily for a smartwatch; shown in Figure 3) lets the user keep the watch naturally worn on the preferred-side wrist – no need to relocate the watch upon changing the exercise type. The ***signage mode*** (primarily for a smartphone; shown in Figure 5) lets the user mount the phone in front of them so that they can naturally see the display while exercising. Both modes provide real-time exercise classification and repetition counting via auditory feedback [66, 67, 115], while the signage mode adds visual feedback and even allows other apps to run in the foreground, e.g., YouTube or a self-monitoring & guidance app [76, 130]. In essence, ProxiFit keeps the natural way of using each device throughout an entire exercise routine. Also, obviously ProxiFit does not require external instrumentation. This makes ProxiFit **satisfy conditions (3) and (4)** in the problem statement. Our supplemental video demonstrates the real-time operation of ProxiFit at an actual gym in both wearable and signage modes.

Building ProxiFit with high usability and robustness to be deployable in real gyms faces multiple challenges. First, the magnetic disturbances around unmagnetized iron are extremely weak [37, 88]. In ProxiFit, it is worsened by the moving parts of a machine being apart from the device, often 0.6+ meter. Weak signals result in highly inconsistent signatures even for same-path repetitions, as shown in Figure 9. This phenomenon causes many feature extraction and classification techniques to fail. Another challenge is that the magnetic disturbances are unique to each machine instance, not to the machine type, as the magnetic signature is engraved at metal annealing [27, 38, 45]. This rules out typical training strategies – train a general model with a large dataset for each machine type and apply it everywhere for classification. Instead, the training must be done *per every instance* of exercise machines, severely multiplying the training workload. To keep ProxiFit practical, the per-instance training must be greatly simplified yet still effective.

We present step-by-step development of ProxiFit, turning a commodity device as-is into an in-proximity tracker for weight exercises, under the harsh challenges of extremely weak magnetic signature and simple-training constraints. We extensively search for robust, lightweight models that are neither susceptible nor overfit to weak and erratic magnetic disturbances. Also, we make the overall design of ProxiFit be conditioned to our unique ***single-person training*** policy. For an unseen instance of an exercise machine, the training is quickly done *only with a handful amount of data collected from a few trials performed by* ***a single person***, likely the gym administrator testing a newly installed machine for the first time. Then, the model serves everyone else. Note that this single-person training is opposite to (and a lot more challenging than) the popular LOOCV (leave one out cross-validation–trained with $N-1$ people and tested to the remaining 1). Below we list our self-defined terminology frequently referred to throughout this paper.

We implement ProxiFit to be cross-device compatible between an iPhone and an Apple Watch. ProxiFit has been extensively evaluated with a total of 19 users, at 3 different gyms featuring 5 different brands, on 5 types of lower-body machines, 4 types of free-weight exercises, and 5 types of upper-body machines, in both wearable

[1]For demonstration, please watch the supplemental video submitted together with this paper.

Terminology	Description
$\mathcal{M}$-	Prefix denoting that the sensor is in motion.
$\mathcal{S}$-	Prefix denoting that the sensor stays still.
$\mathcal{M}$-*Exercise*	An exercise involving the motion of the sensor, *for a given sensor placement.*
$\mathcal{S}$-*Exercise*	An exercise **not** involving the motion of the sensor, *for a given sensor placement.*
$\mathcal{M}$-*Free-weight*	A free-weight exercise where the very arm wearing the device is actively exercising.
$\mathcal{S}$-*Free-weight*	A free-weight exercise where the other arm (not wearing the device) is actively exercising.
Single-person training	Our training policy that trains with only 1 person, tests with the remaining $N-1$ people.

Table 1. List of wearable exercise tracking systems

Work	Method	Sensor placement	Holistic coverage	Works on *single* COTS	Instrumentation -free	Supports $\mathcal{S}$-*Exercise*
ProxiFit (wearable)	Acc+Gyro+Mag	Wrist	O	O	O	O
ProxiFit (signage)	Mag	Holder	O	O	O	O
Chang et al. [32]	Acc	Hand, waist	X	X	O	X
RecoFit [99]	Acc+Gyro	Arm	X	O	O	X
MiLift [120]	Acc+Gyro	Wrist	X	O	O	X
Soro et al. [121]	Acc+Gyro+Mag	Wrist, ankle	O	X	O	X
Velloso et al. [125]	Acc+Gyro+Mag	Hand, waist, arm, dumbbell	O	X	X	X
MyoGym [80]	EMG+Acc+Gyro+Mag	Arm	X	O	O	X
Bian et al. [29]	Capacitive coupling	Wrist	O	X	O	O
ERICA [115]	Acc+Gyro	Ear, dumbbell	O	X	X	X

Acc: Accelerometer, Gyro: Gyroscope, Mag: Magnetometer, EMG: Electromyogram

and signage modes. We rigorously evaluate the robustness of ProxiFit over many dimensions: long-term stability of magnetic signature, influence from weather conditions or user physiques, possible magnetic interference between nearby machines, etc.

§2 lays out the backgrounds, taxonomy of prior works, and positioning of ProxiFit. §3 overviews the architecture; §4 through §7 detail the challenges and experiment-driven development. §8 and §9 shows our implementation and evaluations. §10 explores extending magnetic sensing towards $\mathcal{M}$-*Exercise*. §11 discusses open issues.

2 BACKGROUND, RELATED WORKS, AND MOTIVATING EXPERIMENTS

2.1 Demand for Pervasive Exercise Monitoring

Studies report that pervasive tracking of exercise is beneficial as it motivates to lose weight [30, 53, 109], reduces blood pressure [78], and keeps users more active in general [111]. However, manually logging exercises is cumbersome and users may forget the details after exercises. Multiple research prototypes accommodate such needs, and surveys reveal users find such applications to be helpful and prefer using one over manual logging [64, 68, 84, 120, 125]. Exercise tracking apps such as Gymatic Workout Tracker [16], Garmin [12], and Coros [11] commercialize long-researched topic on smartwatches and smartphones. Gymatic Workout Tracker with 1900+ reviews at an average of 4.3/5.0 rating proves its popularity.

2.2 Exercise Monitoring Systems on Wearables

The motion-sensing nature of IMU and wearables make a perfect combination for exercise monitoring [40, 41, 44, 81, 100, 107]. A survey reports strong user preferences toward a wrist-worn device. MiLift [120] is one of such, implementing the application on a commercial Android smartwatch, and achieving an accuracy of 97.5%

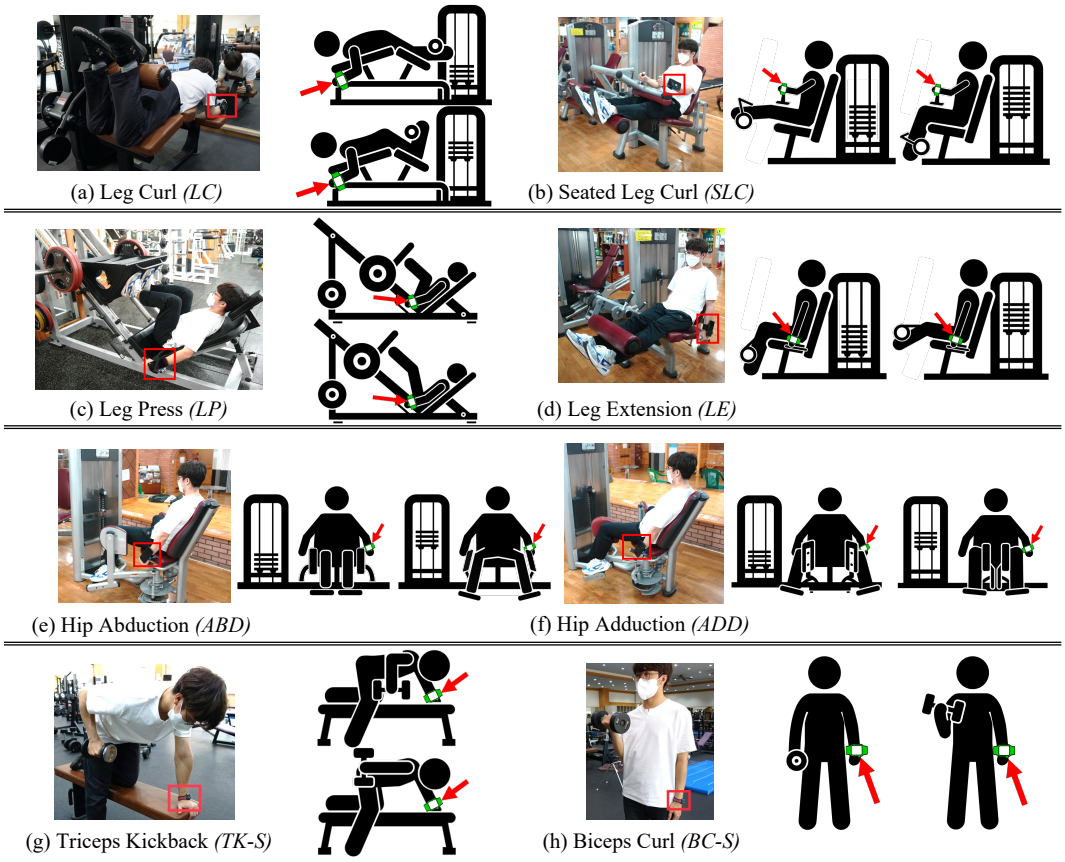

Fig. 3. Illustration of major $\mathcal{S}$-**Exercise**s at typical gyms, for a wrist-worn wearable device. Each exercise is paired with pictograms depicting its dynamics. Red bounding boxes and arrows indicate the device.

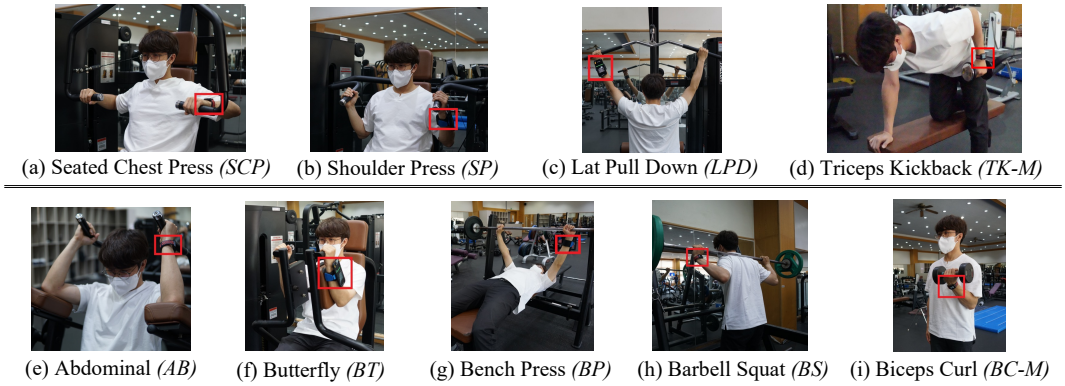

Fig. 4. Illustration of major $\mathcal{M}$-**Exercise**s at typical gyms, for a wrist-worn wearable device. Red bounding boxes indicate the device.

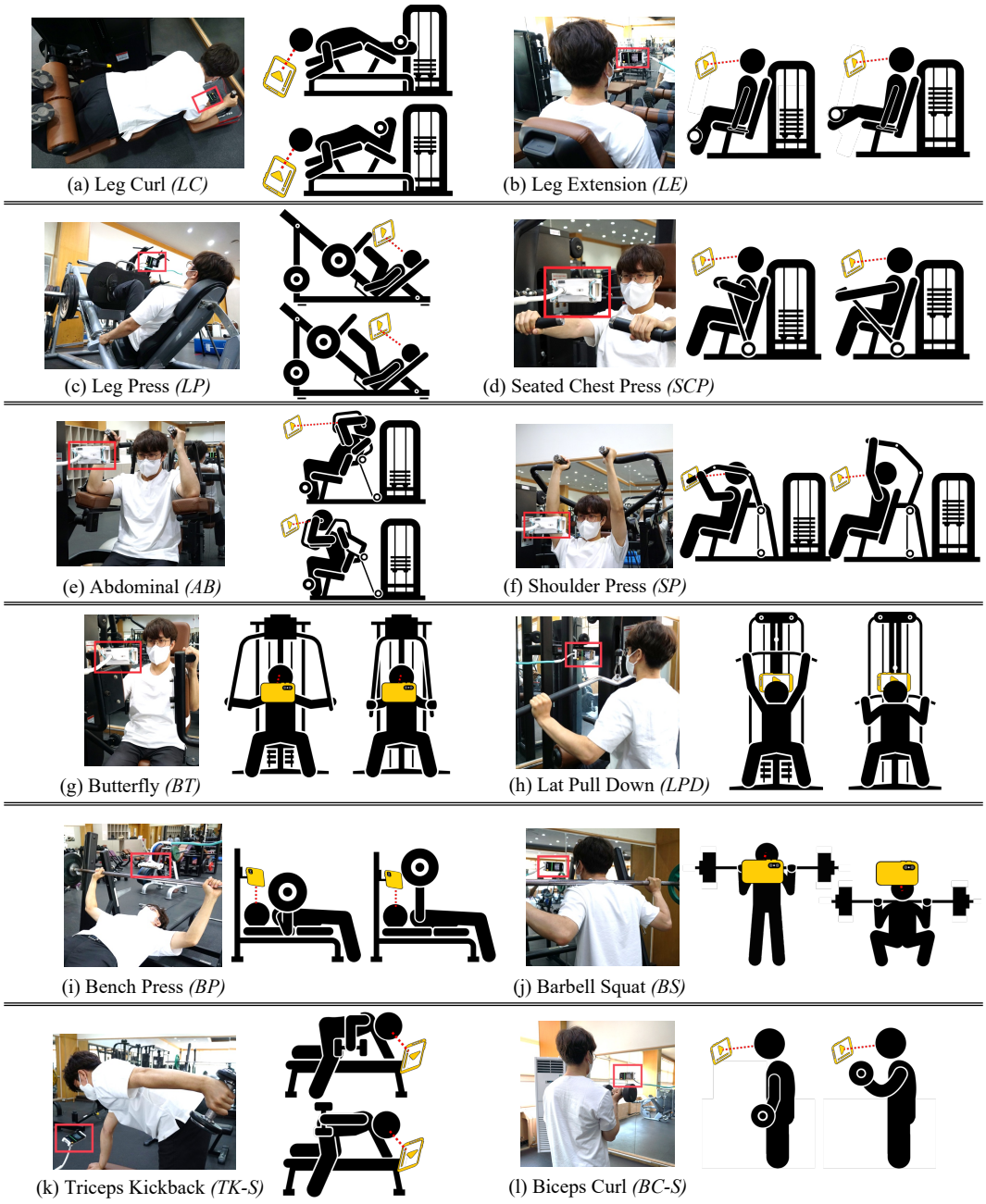

Fig. 5. ProxiFit in signage-mode applied to major weight exercises. Red boxes and yellow icons indicate smartphones. Note that every exercise is treated as $\mathcal{S}$-*Exercise* here, as the device always stays still.

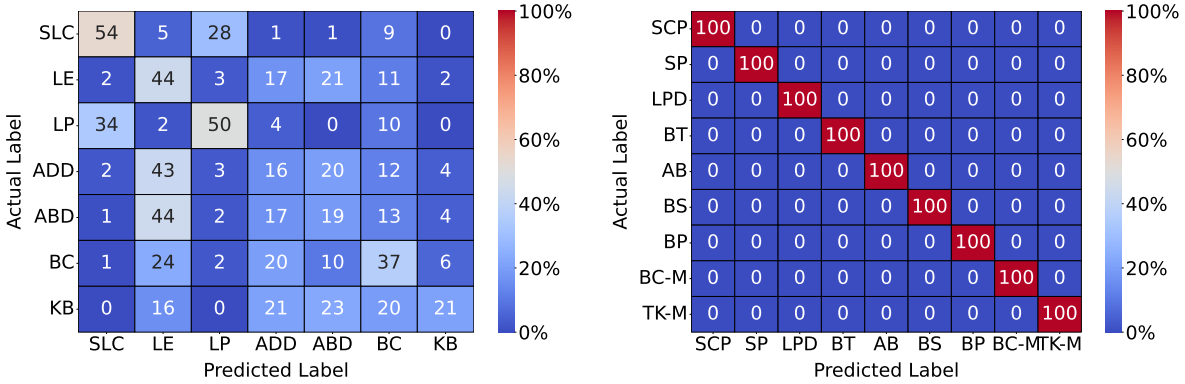

(a) Confusion matrix showing very poor classification accuracy (%) of MiLift on $\mathcal{S}$-*Exercise*

(b) Confusion matrix showing perfect classification accuracy (%) of MiLift on $\mathcal{M}$-*Exercise*

Fig. 6. Verifying a gravity-based approach (MiLift) on lower-body weight machines using a wrist wearable. There exist machines with similar postures, resulting in poor results. (35.9%)

in classifying 15 weight exercises. Unfortunately, IMU-based systems' outstanding accuracy applies only to $\mathcal{M}$-*Exercise*; they are fundamentally incompatible with $\mathcal{S}$-*Exercise*s as mentioned in §1. One may argue that IMU-based methods could detect $\mathcal{S}$-*Exercise*s since the user's wrist may twitch while exerting large force on other limbs. To verify, we tested MiLift [120] on various exercises including $\mathcal{S}$- and $\mathcal{M}$-*Exercise*s. Figure 6 reveals MiLift struggles on $\mathcal{S}$-*Exercise*s, in contrast to $\mathcal{M}$-*Exercise*s. We also tested $\mathcal{S}$-*Exercise*s on the Gymatic Workout Tracker app which can register an unseen exercise by recording 3+ repetitions. This app was unable to register any of leg curl, leg extension, and leg press – all $\mathcal{S}$-*Exercise*s. Possible alternatives to bring full-body exercise tracking to wearables are mostly limited to locality sensing. One strategy is to deploy multiple IMU sensors at multiple limbs [32, 63, 103, 122, 131] and even to dumbbells [125]. However, requiring multiple wearables is financially unattractive. Another strategy is to relocate the smartwatch to the body position [73] being exercised, which is inconvenient and against the natural way of wearing a smartwatch. Exotic sensors, such as electromyograph (EMG) [60, 80, 98], electric skin potentials [77], or textile [23, 132] opened new modality in exercise tracking, but their sensing scope still remains local; lower-body exercises are not sensible from the wrist. A body capacitance sensor as a single wrist wearable [29] was developed, bringing full-body exercise tracking. But the consistency of sensing is low for practical use. Moreover, requiring a non-commodity sensor that most people do not have poses a fundamental limitation against market share.

Table 1 catalogs wearable exercise monitoring systems based on our practicality conditions (1) through (4) in §1. Despite novel and multifaceted approaches, a single system satisfying all conditions is yet to be devised.

2.3 Exercise Monitoring Systems on Smartphones

Pernek et al. [110] proposed two ways of enabling a smartphone to track gym machine and free-weight exercises: putting the phone on the weight stack of the gym machine, or wearing the phone with an armband for free-weight exercises. Both practices lie on the common principle – making the device move along exercises. Khan et al. [71] used up to three smartphones attached to the forearm, waist, and thigh to bring full-body exercise tracking. However, the three-phone requirement makes it less practical. Fu et al. [54, 55] suggested acoustic Doppler sensing to detect nearby activities. However, susceptibility to multi-paths and background noises in crowded gyms [128] would limit its deployability at gyms.

2.4 Exercise Monitoring Systems by Instrumenting Gyms or Equipment

Instrumenting gyms or equipment has long been a parallel alternative to COTS approaches [20, 65, 106, 108]. W8-Scope [114] instruments the machine's weight stack with a sensor, making it travel up and down affixed to the moving weight stack. ERICA [115] takes a hybrid approach using both 'earable' and dumbbell-attached sensors. Other external instrumentation approaches utilize Wi-Fi [56, 126], camera vision [39, 43, 50, 59, 69, 72, 124, 129], VR [113], RFIDs [47], LiDAR [117], and floor mats [123].

We address that sensing from either infrastructure or user-owned devices is an apple or orange problem. Each exhibits unique pros and cons in terms of location-dependency, initial investment, beneficiary user pool, and supported sensing modes. In addition, continuous vision or sound approaches raise privacy concerns. Thus, a single all-time winner is unlikely. User-owned wearable approaches deserve appreciation for their own merits.

2.5 Magnetic Sensing: Basic Principles and Use Cases

It is known that magnetometer readings exhibit spatially erratic but temporally stable distortions in the vicinity of iron objects [42, 127]. Ferromagnetic materials such as iron are either magnetically soft or hard. Soft materials are not magnetized by themselves. But, upon applying external magnetic fields (including geomagnetism), the electron spins are aligned [101], exhibiting its own magnetic field also known as soft iron distortion. Iron objects' magnetic properties are largely set at manufacture time; heating and annealing form 'domains'–tiny regions with aligned electron spins [45]. The magnetism of neighboring domains may not perfectly cancel out but yield a non-zero field known as spontaneous magnetization [27, 38], having the object act like an irregular-shaped group of very weak permanent magnets. As a result, a weight machine or equipment as an iron-rich object causes combined disturbances where the geomagnetism, machine geometry, and material/manufacture variances contribute altogether.

Ambient magnetic field sensing based on a commodity mobile device has been studied for real-life problems, e.g., indoor localization [25, 42, 48, 49, 89, 112, 118, 127], NFC [104], and daily hygiene [62]. MagAttack [37] and MagHacker [88] address new cyber-physical vulnerabilities that magnetic sensing opens. Instrumenting an object with a permanent magnet has enabled driver monitoring [61] and natural user interfaces [26, 33–35, 58, 90, 91, 93, 105].

Among others, Mago [36] senses the periodic spin of vehicles' wheels to detect the transport mode, which is relatable to sensing periodic repetitions of unmagnetized iron mass in ProxiFit. Mago shows decomposing magnetic signals for high-level analysis is infeasible, and opts for intensity-based frequency analysis. We re-confirm such infeasibility. Furthermore, we find intensity-based features are not reliable enough for ProxiFit to effectively address its increased complexities – e.g., higher degrees-of-freedom of the weight machine dynamics, the structural uniqueness of each machine type, and even the instance-unique magnetic signature. §6 devises new, invariant features to tackle the problem.

3 PROXIFIT SYSTEM OVERVIEW

We introduce ProxiFit, a single commodity device system (*either* a smartwatch or a smartphone) that newly enables proximity magnetic sensing to track a holistic family of weight exercises. Utilizing intrinsic magnetism of iron-rich weight machines & equipment, ProxiFit brings support to $\mathcal{S}$*-Exercise*s, i.e., 'lower-body weight machines' and 'free-weight lifting by a non-device-worn arm'. To our knowledge, this has not been supported by a single, naturally-worn, commodity COTS wearable, as detailed in §2 and the problem statement in §1. ProxiFit also premieres the signage mode (Figure 5)– letting the device off-body to offer a natural line-of-sight on the phone's display while exercising.

ProxiFit is highly practical; it is widely deployable, user-friendly, and of little cost. ProxiFit uses only a single, user-owned, unmodified commodity device, e.g., a phone or a watch, and works in uninstrumented gyms.

Specifically, (1) ProxiFit works from day 1 for anyone without per-user training. (2) It lets the device be naturally worn on the wrist or naturally in front of the user. (3) It works automatically through the user's entire gym routine – entering a gym, sitting on a machine, performing repetitions, taking a break, doing a different exercise, walking around, etc.

3.1 ProxiFit Architecture

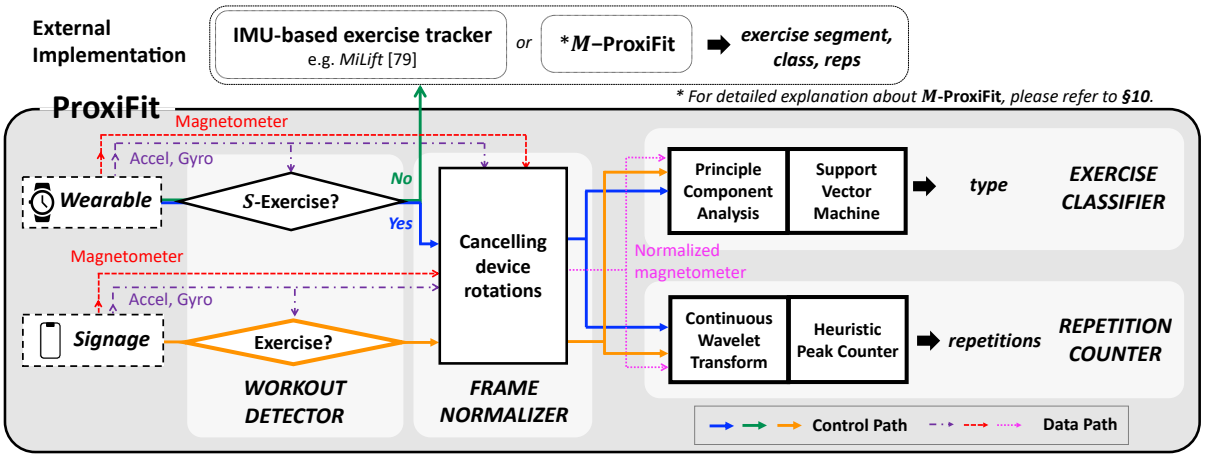

Fig. 7. ProxiFit System Architecture illustrating major components. Solid lines represent control paths; dashed/dotted lines represent data paths with the annotations of which sensor data flows along.

Figure 7 illustrates the overall architecture (best viewed in color). The control paths and data paths are separately shown. The processing paths are partially different depending on wearable or signage mode, and extend to an external delegate module such as MiLift [120] or $\mathcal{M}$-ProxiFit (see §10) for processing of conventional $\mathcal{M}$-*Exercises*. On a single device (either a watch or a phone), ProxiFit senses from magnetometer, accelerometer, and gyroscope. We apply a sliding window on the sensor streams to process the data. Our exercise data reveals single repetition can take 0.8 to 2 seconds. A larger window size, due to more samples, typically results in better accuracy at the cost of more computation and delayed response. We choose a 3-sec window (at a stride of 0.5-sec) to make sure at least a single whole repetition is captured while reducing the latency. The accelerometer and gyroscope are used for preprocessing and filtering; exercise classification is done solely using the magnetometer.

In the wearable mode, the *workout detector* employs accel- and gyro-based thresholding to determine if the current sensor streams fall in $\mathcal{S}$-*Exercise*. Non-$\mathcal{S}$-*Exercise* is passed to the external module, which determines whether it is $\mathcal{M}$-*Exercise* or not an exercise at all. In the signage mode, inertial features are not informative as the device always stays still. Thus, thresholding is replaced with a decision tree classifier with autocorrelation. §4 details the workout detector.

Detected sensor streams of workouts go through the *frame normalizer*, which transforms the sensor data into a constant external frame of reference in real-time. This is necessary to nullify the magnetic artifacts due to slightly different device poses or user physiques. §5 elaborates on the frame normalizer.

The *exercise classifier* classifies the current exercise into a known type. It has two pre-trained models, for wearable and signage modes, respectively. §6 explains the classifier, along with our feature set and single-person training policy.

The *repetition counter* takes magnetic sensor data, and inspects frequency-domain features over a continuous time with continuous wavelet transform (CWT) to distill periodic trends out of the faint magnetic disturbances.

Finally, repetition is counted in real-time by peak counting on the frequency feature with the most consistent repetitions. Unlike the classifier, the repetition counter has only a single instance that serves all usage modes and exercise categories; there are no case-dependent hyperparameters. §7 explains our design of repetition counter.

3.2 Datasets

Table 2. Summary of datasets

Mode (device)	Dataset	Location	Exercise categories	No. of participants	Participant height (cm)	Participant weight (kg)	Exercise weight (kg)	Participant age	Total duration (h)
Wearable (phone)	$\mathcal{D}_1$	Gym_{univ}	**Upper** {SCP, SP, LPD, BT, AB} **Lower** {LC, LE, LP} **Free-weight** {BS, BP, BC, TK}	15	162–185	53–100	4.4–80	22–31	21.4
	$\mathcal{D}_2$	Gym_{ExtA}	**Lower** {SLC, LE, LP, ADD, ABD}	9	169–180	56–95	5–55	24–31	11.6
	$\mathcal{D}_3$	Gym_{ExtB}	**Lower** {LC, LE, LP}	5	169–180	70–95	15–40	25–31	4.9
Signage (phone)	$\mathcal{D}_4$	Gym_{univ}	Same as $\mathcal{D}_1$	9	162–181	53–95	2.2–30	23–31	8.9
Wearable (watch)	$\mathcal{D}_5$	Gym_{univ}	**Upper** {SCP, SP, LPD, BT, AB}	6	169–181	70–95	5–30	25–31	2.5
	$\mathcal{D}_6$	Gym_{ExtA}	**Lower** {SLC, LE, LP, ADD, ABD}	5	169–180	70–95	5–25	25–31	5.9

We summarize the exercise datasets to which are referred along with the design and evaluation process. Table 2 lists 6 datasets: $\mathcal{D}_1$ through $\mathcal{D}_6$. The whole datasets involve a total of 19 users (2 F & 17 M), at 3 different gyms, over 14 months period, both wearable and signage modes, covering 14 exercise types including lower-body machines, upper-body machines, and free weights. The gyms are chosen to diversify the exercise equipment's brands to ensure the datasets' generality. In each dataset, each participant performed 10 sessions per exercise type in that dataset. (1 session = 10 repetitions) Some datasets are small in size to abide by the access regulation as per the COVID situation. In every data collection, we kept the gym environment as-is while allowing subjects to freely plan their exercises – the order of exercise, machine adjustments, weight, and pace. Note that Gym_{ExtA} and Gym_{ExtB} are public gyms; data is collected during business hours under interference from other users. The following sensor streams were collected at 100 Hz: magnetometer, accelerometer, gyroscope, and attitude (device orientation) through iOS's `CoreMotion` APIs. We video-recorded every data collection for labeling ground truths. All experiments were conducted under IRB approval.

The sensor data were collected from either an iPhone 12 Pro or an Apple Watch Series 6. For the signage mode, we collected the data only from the phone ($\mathcal{D}_4$), as the display size would matter to ensure natural, comfortable viewing in signage mode. For the wearable mode, we have three datasets from a phone ($\mathcal{D}_1$ through $\mathcal{D}_3$) and two datasets from a watch ($\mathcal{D}_5$ & $\mathcal{D}_6$). In $\mathcal{D}_1$ through $\mathcal{D}_3$, the phone was strapped on the user's wrist so that it can sense in the same pose as a watch, as shown in Figure 3(a)-(f) and also in our supplemental video submission.

The reason for using a phone to mimic a watch is due to Apple's aggressive scheduling in watchOS; it suspends background workout tracking depending on CPU usage [17]. We observed our sensing app being abruptly killed in the middle of exercise sessions, making continuous data collection very unreliable. For this reason, we collected most large-sized datasets from the phone being worn like a watch. From the watch, we managed to collect two usable datasets ($\mathcal{D}_5$ & $\mathcal{D}_6$) which are smaller in size and coverage. We use $\mathcal{D}_5$ and $\mathcal{D}_6$ to demonstrate ProxiFit is seamlessly usable with a watch, verifying our system is not biased to the phone. We clarify that this is *not a technical shortcoming in a fundamental sense*, but rather Apple's proprietary policy; it could be resolved once Apple lifts the bar.

3 different gyms are covered in our datasets to demonstrate ProxiFit's cross-gym portability. Gym_{univ} is our university gym; Gym_{ExtA} and Gym_{ExtB} are two external gyms, respectively. Each gym has different brands of weight machines:'Matrix' and 'Lexco' in Gym_{univ}, 'Dynaforce' and 'Life Fitness' in Gym_{ExtA}, 'Newtech' in Gym_{ExtB}, supporting ProxiFit's generalizability to machine variety. The external gyms were far more crowded than Gym_{univ},

Table 3. SNR analysis on 6 types of $\mathcal{S}$-*Exercise*s. Parenthesized ranges indicate (min, max).

		LC	LE	LP	ABD	ADD	SLC
Idle state	DC offset (uT)	97.30 (94.21–99.00)	38.98 (35.99–41.28)	34.92 (33.52–36.00)	73.38 (41.77–108.50)	38.17 (28.41–48.64)	50.93 (48.83–54.35)
	AC intensity ('noise') (uT)	0.35 (0.31–0.39)	0.31 (0.28–0.33)	0.34 (0.30–0.37)	0.35 (0.29–0.46)	0.31 (0.28–0.33)	0.33 (0.29–0.37)
$\mathcal{S}$-*Exercise* being performed	Envelope amplitude in a single repetition ('signal') (uT)	0.65 (0.48–0.93)	0.41 (0.36–0.48)	1.23 (1.08–1.53)	1.93 (1.55–2.36)	0.96 (0.85–1.07)	0.58 (0.42–0.90)
	SNR (dB)	5.09 (2.55–7.97)	2.48 (0.91–4.82)	11.01 (9.53–14.19)	15.33 (13.76–17.36)	10.10 (8.23–11.64)	4.69 (2.12–8.11)

reflecting more real factors. To make the best use of fewer data collection chances from regular business hours of Gym_{ExtA} and Gym_{ExtB}, we focused on their lower-body machines, because: (1) Gym_{ExtA} & Gym_{ExtB} owned a more variety of lower-body machines (5 & 4 types, respectively) compared to Gym_{univ} (3 types); Figure 3(b), (e), (f) are the lower-body machines unique to Gym_{ExtA}. (2) the lower-body machines are one of our unique addition to the relevant literature.

4 WORKOUT DETECTOR

To make ProxiFit intervention-free, it should auto-detect active exercise sessions along the user's natural gym routine. The workout detector is the only component that runs for an entire routine, strongly favoring a lightweight detector [82, 83].

Detecting a target segment out of a continuous signal is often done by searching for some characteristic signatures. Unfortunately, $\mathcal{S}$-*Exercise*s rarely leave useful acceleration signatures as showcased in §2.2. Magnetometers, although capturing more information than accelerometers, either could not be a drop-in replacement due to inherent limitations.

Profiling ambient magnetic disturbances from $\mathcal{S}$-*Exercise*. Table 3 lists our measurements from the wrist-worn device of the user performing 6 types of $\mathcal{S}$-*Exercise*s. Firstly, the table breaks the idle-state ambient magnetic field into the DC offset (largely geomagnetism) and the AC intensity (considered 'noise'). The idle-state indicates the user holding the handle still but not performing repetitions. Next, we measure the envelope amplitude that the ambient magnetic field swings during a single repetition period (considered 'signal'), and calculate the signal-to-noise ratio (SNR). We report the mean values along with the min-max ranges, from 20 measurements per machine. As the magnetic field is a 3-D vector quantity, we take the L2-norms and average them to represent the mean levels of noise and signal. The mean SNR ranges from 2.48 dB to 15.33 dB, depending on the machine type. Also, we need to ensure that the sensor precision is good enough to detect signals at such amplitudes. Although the magnetometer model on iPhone 12 Pro is not publicly known, we make an educated guess based on the reports: (1) iPhone 6s has the magnetometer model of HSCDTD007 with 0.15 uT precision, made by ALPS [36], (2) all iPhones from 6s through 8 plus use a magnetometer from ALPS [92], (3) iPhone 13 pro has ALPS HSCDTD00xA series magnetometer [5], and (4) ALPS currently lists only one geomagnetic sensor product (HSCDTD008A) [9, 13] of 0.15 uT precision. Given the consistent 0.15 uT precision of the magnetometer product family in iPhone models preceding and succeeding iPhone 12 pro, we speculate that iPhone 12 pro's magnetometer precision is likely 0.15 uT, too. It is unlikely a serious issue given the signals' scales in Table 3.

Detecting $\mathcal{S}$-*Exercise*s. Despite the positive SNR, the challenge to detect the presence of an $\mathcal{S}$-*Exercise* is that magnetometer readings are a combination of ambient magnetic field variation and sensor displacement. Sadly, the impact of sensor displacement (e.g., the user naturally moves) is not negligible compared to repetition-induced

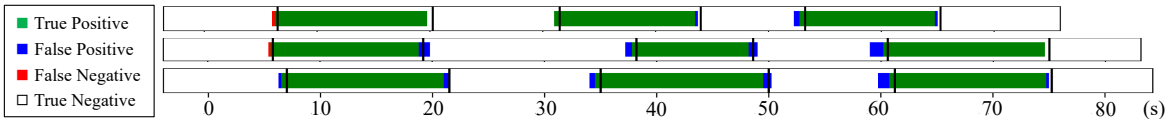

Fig. 8. Detailed view of detected $\mathcal{S}$-*Exercise* segments along a part of continuous gym routines

field variations. E.g., rotating the device by 10° may see a difference as big as 3 uT under a 45 uT offset of the ambient magnetic field.

We take a reverse way that removes unlikely ones instead of finding the repetition-likely. Humans are intolerable to absolute settlement, moving slightly without intent [79]. We note that a user's wrist stays unnaturally still during $\mathcal{S}$-*Exercise*s, to firmly hold the handles or rest on the body in order to properly exert force. In favor of unnaturally still window slices, we set upper-limits to the RMS power of acceleration and rotation rates whereas others are early-rejected. In $\mathcal{D}_1$ this removes 99.7% of non-$\mathcal{S}$-*Exercise*s in a 250-min period and with only 2.7% of false-negatives.

There is a possibility that the device stays stationary but the user is not doing $\mathcal{S}$-*Exercise*s. To prevent such false-positives, ProxiFit necessitates detecting a minimum of three repetitions via the repetition counter before it acknowledges the signal as an exercise, preventing random noise from being detected as an exercise. §7 also elaborates on this filtering.

Analyzing in-situ detection performance. Figure 8 visualizes part of the segmentation results along continuous gym routines containing 3 sessions of 3 different machines and non-exercise movements. Most FPs/FNs appear at either edge of true exercise sessions. To further remove short FP/FNs, we exploit that an exercise session typically consists of 7-15 repetitions. To balance between confidence and responsiveness, we empirically choose 3 samples (1.5 sec).

5 FRAME NORMALIZER

For $\mathcal{S}$-*Exercise*s and signage mode, an exercise-eligible window has to be normalized per its frame of reference to rectify user and instance variations. The frame normalizer corrects deviations by transforming each sample based on its frame of reference, and saves it to a session buffer for the following classifier and repetition counter.

In lower-body machines, the handles force the user's hands to stay in a certain pose, confining the sensing device in a tiny space. A grip is about 13 cm long, and the average hand of adult males is 8.3 cm wide [119], leaving 4.7 cm of freedom which is negligible considering gym machines of at least 50 cm travel per repetition. However, the rotation of devices is not fully controlled: (1) The anatomy of human wrist cross section allow a watch to be rotated by up to $[-30°, +30°]$ [87]. (2) Different physiques in arm lengths and shoulder widths lead users to grip the handles at dissimilar angles. (3) Slight unconscious wriggles may happen upon exerting force.

Consequently, compensating for the subtle device rotations is crucial for sample consistency and model stability. Frame normalizer cancels unintentional rotations by utilizing relative rotations derived from the `device attitude`. Every reference frame supported in Apple API sets the Z-axis to parallel the gravity. While it also supports aligning the X-axis towards the north pole, it is estimated with the magnetometer. ProxiFit is put under a magnetically dynamic situation which may confuse the estimated orientation. Hence the frame normalizer is not applied on the Z-axis to avoid false corrections.

6 EXERCISE CLASSIFIER

While we have explored various advanced methods to classify exercises with ambient magnetic signals, ProxiFit settles for a rather simple Support Vector Machine (SVM) (radial basis functions kernel (RBF) & $C = 70$ (wearable) / $C = 10$ (signage)) with the following 4 features: {Normalized & Raw principal component vector of magnetic

signal, and Normalized & Raw principal component vector of element-wise difference magnetic signal}. In this section, we show our choices outperform others even with training on a few single-person repetition sets per exercise type.

We first focus on the wearable mode in exploring the classifiers. Then, we show the same architecture and training policies are seamlessly applied in signage mode (where every exercise is an $\mathcal{S}$-*Exercise*). Unless specified, the accuracy hereafter is obtained with *single-person training*, i.e., "train on only one person's data, test on everyone else, and average the accuracy over N choices of the training person." This is opposite to and much harsher than 'leave one out cross validation (LOOCV)', but crucial to fight the instance-unique magnetic disturbances and thereby ensure the practicality. §6.1 articulates candidate classifiers and features we tested. Then, §6.2 and §6.3 present the strategy that we settled in.

6.1 Classifier and Feature Search Attempt

Deep neural networks demand large data. Our key challenge is to increase selectivity high enough to classify machines despite SNR as low as 0.91dB. Denoising approaches, which train models with ground truth and noisy counterpart, are inapplicable because (1) the ground truths of higher SNR are not obtainable, and (2) synthetic ground truths are infeasible as the magnetic disturbances are instance-unique, solidified at manufacture time. Another option is to design an end-to-end network and delegate both feature-finding and classification. It increases problem space compared to denoising and thus requires a far more extensive dataset. Unfortunately, growing datasets is against practicality in ProxiFit due to the instance-wise magnetic specificity and the single-person training policy.

We experimented with 1-D CNN [57] and LSTM [102] which are well-recognized in wearable HAR. The 1-D CNN tops at 67.1% even under traditional 8:2 train-test split, not our single-person training. The LSTM achieved 82.8% under the same 8:2 split. Under our single-person training, the accuracy heavily fluctuates around 70% and drops below 50%. We believe that our problem with minimal per-instance training constraint is not favored by data-hungry deep learning.

Computation cost is also important when it comes to a smartwatch app. We tested the battery consumption of LSTM and SVM(rbf) on iPhone 12 Pro. We forced LSTM to run on CPU, as processors in smartwatches do not have deep learning accelerators. After a 60-min classifier run, SVM used 2%p battery while LSTM used 12%p battery. While this battery consumption on a smartphone might seem acceptable, iPhone 12 Pro (10.78 Wh) [4] has a 10x battery of Apple Watch 6 (1.02 Wh) [3]. Thus, running LSTM on smartwatches would severely hamper daily usability.

High noise prevents signature matching. We explored parametric and non-parametric approaches to find closer matches to prerecorded signatures. For parametric, Gaussian Mixture Model marked only 40.5%. For non-parametric, we constructed sample distributions per exercise type, and applied Kolmogorov-Smirnov (KS) test to quantify the similarity of each type. The accuracy was only 15.7%. Figure 9 visualizes 3-D magnetic field trajectory from five repetitions of hip abduction. The plot reveals significant inter-repetition deviations and drifts albeit smoothing. Both results and visual inspection of the signal hint that the distributions across repetitions and sessions are too erratic.

Inflexible statistical features. Now we explore classic feature engineering. We tried popular statistical features – mean, stddev, kurtosis, skewness, interquartile range (IQR), and well-known classifiers – Random Forest, Decision Tree, Naive Bayes, Support Vector Machines (SVMs) with linear and RBF kernels. At first, we searched for the best feature combination on three lower-body machines {*Leg curl, Leg extension, and Leg press*}. We find SVM with RBF kernel performs the best, and {*mean, IQR*} are the most reliable feature combination that marks 81%. We searched the best-performing hyperparameter C from [0.1, 100] range, and kept gamma as 'scale' which is the

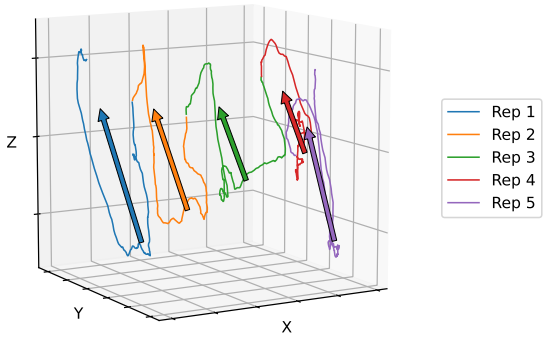

Fig. 9. Raw magnetometer trajectory of five hip abduction repetitions, each visualized with its respective primary component vector. The vector directions are consistent, despite drifts and inconsistency across repetitions.

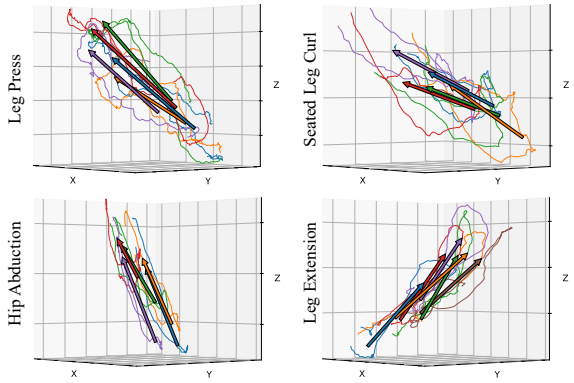

Fig. 10. Each plot visualizes exercise repetitions and their primary component vectors. Primary component vectors are consistent in the same exercise type, but distinguishable with other exercise types.

default for scikit-learn. However, adding two more lower-body machines {*Hip abduction, Hip adduction*}, lowered the accuracy to 65%.

6.2 Principal Component Analysis

Given all inconsistency against stable classification, we focused on distilling the *invariant* across repetitions, sessions, and users, and eliminating everything varies. For $\mathcal{S}$*-Exercises*, we observe that: (a) The magnetism of a machine instance is set at manufacture time. (b) Topological relationship between the moving parts and the handle is constant. (c) Moving parts of a machine follow the same trajectory. (d) But their traveling distance depends on the user's physique. (e) Their traveling speed depends on the user's pace. (f) The amount of moving weight stack depends on the user's choice.

From a stationary magnetometer, its surrounding magnetic field travels as the user performs a repetition. Across different users or weights that may result in (d) – (f), the vector field around the magnetometer may differ. Still, the traveling direction of the surrounding field is consistent for the same machine. To represent the field's traveling direction in a user- and weight-invariant way, we apply principal component analysis (PCA) on the unit vectors of magnetic field samples. Figure 10 shows primary PCA vectors from multiple repetitions for 4 types of exercise. Despite the erratic raw trajectories, the PCA vectors are consistent across the same-exercise repetitions, and distinct across different exercises. Initially, the classifier took all 3 components as input. In-depth inspection discloses that only the primary component suffices, achieving an accuracy of 79.3% using SVM (rbf, C=20). To further elaborate the feature set, the non-normalized principal component vector (i.e., multiplied by its variance) is included in the feature set, to inject how prominent the primary component is compared to the secondary or ternary ones. With two 3-D vectors, the classifier achieved 94.9% on three exercises, and generalizes well to five exercises with 86.2% accuracy.

While the directionality of the signal itself is proven to be reliable and informative, we also find the delta of the directionality to be helpful. Adding both normalized and non-normalized principal components of element-wise difference of raw signal to the feature set, and finally tuning the SVM's hyperparameters C to be 70 (wearable) & 10 (signage), we marked 97.2% accuracy on three exercises, and 94.0% on five exercises.

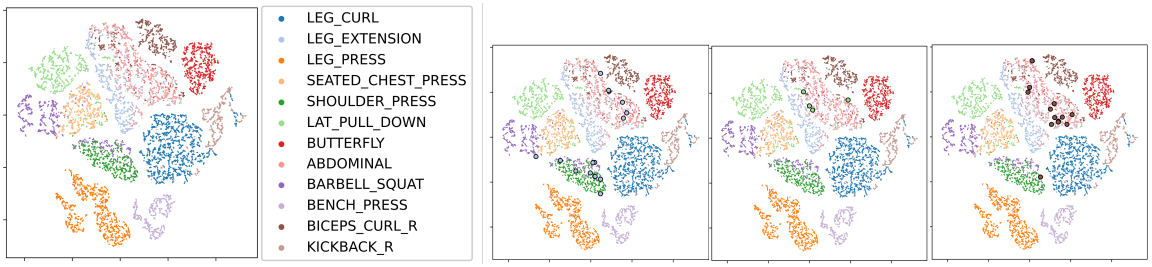

(a) t-SNE of 12 signage exercises (b) Examples of outliers filtered by majority voting

Fig. 11. t-SNE plot for features of 12 signage exercises

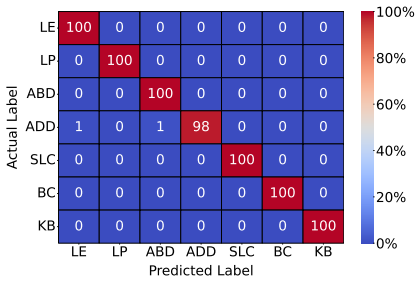

Fig. 12. Confusion matrix of exercise classification (%), at single-person training and with majority voting (average 99.7%)

6.3 Majority Voting

So far, we reported the classification accuracy on a per-window basis (3-sec-long, similar to a typical repetition), which is sensitive to outlying repetitions; users may see momentary misclassifications during a session. The nature of weight exercises dictates only one exercise type exists during a session – the machine that the user is on. Thus we apply continuous majority voting, which hides the momentary misclassifications and improves the user-perceived accuracy. Figure 11a is a t-SNE plot of our feature vectors on 12 signage exercises, illustrating our features are mostly well-distinguished between exercises. But some outliers exist, as highlighted in Figure 11b. Further analysis reveals they are minority windows during a single exercise session, impacting per-window accuracy. The majority voting effectively filters them out. Figure 12 describes accuracy after majority voting, where the combined accuracy is 99.7%.

7 REPETITION COUNTER

ProxiFit counts the exercise repetitions in real-time, in parallel with the classification as shown in Figure 7. The repetition counter is *independent* from the classifier; the real-time counting is not delayed by the classifier's post-processing.

We labeled repetitions in 20 randomly sampled workout sessions of $\mathcal{D}_1$ for the ground truths. The repetition counter examines only the primary component as noise overwhelms the information gain at the 2nd+ PCA components. Still, the signals exhibit nontrivial low-frequency fluctuations and high-frequency noise, as shown in Figure 13a. Frequency domain filters are of limited usage here. Repetitions are rather at a low frequency, around 0.3 Hz, which interferes with slow ambient fluctuations. A high-order filter may sharply separate both but introduces a delay in counting.

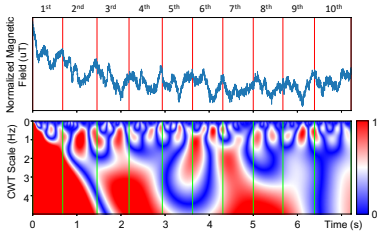

(a) Original signal and its continuous wavelet transform (CWT) result. Erratic behaviors are noticeable in CWT results.

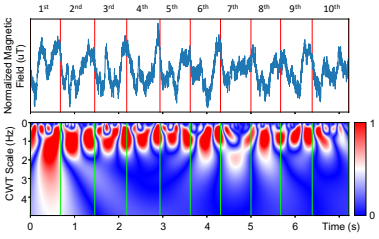

(b) Filtered signal and its continuous wavelet transform (CWT) result. Erratic frequency components are removed with a Butterworth filter.

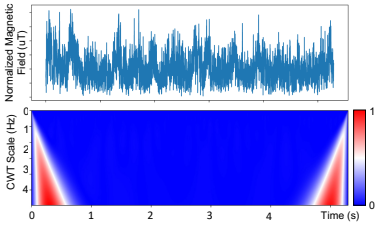

(c) Signal of a person holding a handle without exercising

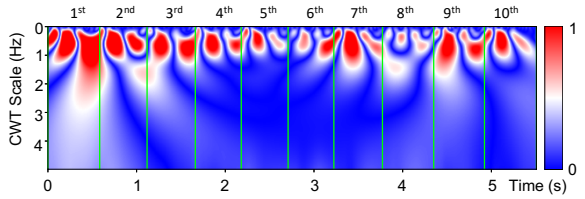

(d) Exemplary CWT of noisy signal. Choosing the correct scale to count peaks is important for accurate repetition counting, as a different scale would have largely different peaks alongside the time axis.

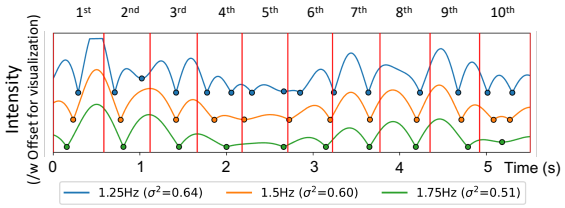

(e) 1-D plot at given CWT scale 1.25, 1.5, and 1.75 each on (d). Normalized variations between peaks are 0.64, 0.60, and 0.51 each. Circles indicate detected negative peaks (valleys).

Fig. 13. Continuous wavelet transform (CWT) of signal and its analysis. Red or green vertical lines denote ground truth repetitions.

We empirically choose a 2nd-order highpass Butterworth at 0.2 Hz for a balance between noise rejection and saving the signals. Figure 13b shows the signals after filtering. Despite cleansing, systematic repetition counting is still unreliable. Peak counting turned out to be heavily parametric to the ground truth samples. Having it fit on 20 sample sessions gives a high average error of 5.56 reps per 10-rep session when evaluated on the entirety of $\mathcal{D}_1$.

To design a counter that adapts to user variation, we apply continuous wavelet packet transform (CWT) to the target signals. Figure 13d reveals the importance of choosing a proper scale (i.e., y-axis). Rough estimations of repetitiveness in a given CWT could be to find two red droplets per repetition. Our repetition counter dynamically finds the best scale for each segment by counting peaks over a plausible scale range, and choosing the most regular-paced one.

We set the automatic scale search range as [0.25, 2] Hz (at 0.25 increment), based on our statistics that a single repetition takes 0.8 to 2 seconds. As an example, Figure 13e illustrates the cross-sections at three different scales on Figure 13d – 1.25, 1.5, and 1.75 Hz. Here, 1.25 Hz shows a couple of false peaks, and 1.5 Hz shows a single false peak at the last repetition. Our algorithm chooses 1.75 Hz as it exhibits the least normalized variance (0.51) of peak intervals. Indeed, we can confirm 1.75 Hz is free of false peaks. Overall, evaluation on $\mathcal{S}$-*Exercises* in $\mathcal{D}_1$ reports accurate counts at a much lower average error of 1.22 rep per 10-rep session despite faint, irregular signal.

Sometimes, an arbitrary segment may be detected as a workout despite users not exercising. One such plausible scenario is when the user is holding the handle firmly, but not exercising yet. Upon such a false-positive segment passing the workout detector, the classifier may make a false guess. To mitigate it, the repetition counter also functions as a gatekeeper for exercise registration, rejecting false-positive segments that do not include at least

three consecutive repetitions. Figure 13c visualizes such signals. Unlike Figure 13b and 13d, the signal is mainly of high-frequency noise. No periodic signature is detected at a low CWT scale level, thus not counting repetitions and preventing a false segment.

8 IMPLEMENTATION

We implemented a ProxiFit prototype in Swift on an iPhone 12 Pro on iOS 15.1 and an Apple Watch Series 6 on watchOS 8.3. While ProxiFit is portable across iPhone and Apple Watch, we mainly used smartphones for major long-running wearable mode experiments due to the aforementioned scheduling limitations, which are not fundamental limitations but a policy set by Apple. Instead, we justify appropriating a smartphone as a smartwatch with short running experiments (§3.2). Signage mode used the phone version as it ensures natural and comfortable viewing.

ProxiFit adopts efficient programming strategies for battery-saving. Sensor values are saved to a circular queue, buffered segments are reused to construct overlapping windows avoiding unnecessary memcopies, and basic statistics are computed on-the-fly. For compute-intensive SVM and CWT, efficient C implementations [19, 31] are linked to Swift, and we use AIToolBox [8] to further accelerate PCA with vDSP vector instructions. We also included an implementation of MiLift [120] to demonstrate ProxiFit can be integrated with other exercise tracking systems to support $\mathcal{M}$-*Exercise*s.

9 EXPERIMENT

From §4 through §7 we discussed module-wise metrics. To assess the deployability of ProxiFit in real gyms, evaluating under various reality factors is imperative. This section presents our evaluations to answer the following questions:

- **End-to-end** (§9.1) : autonomous operation in a gym routine.
- **Signage** (§9.2) : performances in all 3 exercise categories.
- **Watch** (§9.3) : seamless operation with a watch wearable.
- **Portability** to other gyms (§9.4), of:
  - System and hyperparameters (model retrained per gym).
  - Trained model upon same-type machines in other gyms.
- **Runtime** (§9.7) : workload and resource consumption.
- **Robustness** ((§9.6) against:
  - Weather-borne variations (e.g., humidity, lightning).
  - User-dependent variations (e.g., physique, pace).
  - Spatial displacement in free-weight.
  - Spatial displacement / rotational tilt in machines.
  - Magnetic interference between adjacent machines.
  - Magnetic interference around machines.
  - Longitudinal aging of intrinsic magnetism.
  - Using different dumbbells in free-weight.

9.1 Through an End-to-end Gym Routine

We assess the realistic usability of ProxiFit along the users' natural gym routine – lifting multiple weight machines one after another as well as taking breaks in between. We recruited 10 users. Each user stayed for an average of 18 minutes at the gym. Due to the COVID restrictions, we were not allowed to keep them much longer. Although shorter than typical gym routines, we believe the results would be generalizable to a longer stay.

During their stay, each user was asked to naturally do exercise on a total of 14 weight exercises (5 lower- and 5 upper-body machines, 2 barbell free-weight exercises, plus two dumbbell free-weight exercises which are counted twice as $\mathcal{M}$-*Free-weight* and $\mathcal{S}$-*Free-weight* depending on which arm the exercise is done), one after another. Each user performed a 10-rep session on each exercise. We let them do freely between sessions, e.g., taking a rest, walking around, doing chit-chats. The gym-routine data on which we assess ProxiFit includes all of these uncontrolled activities.

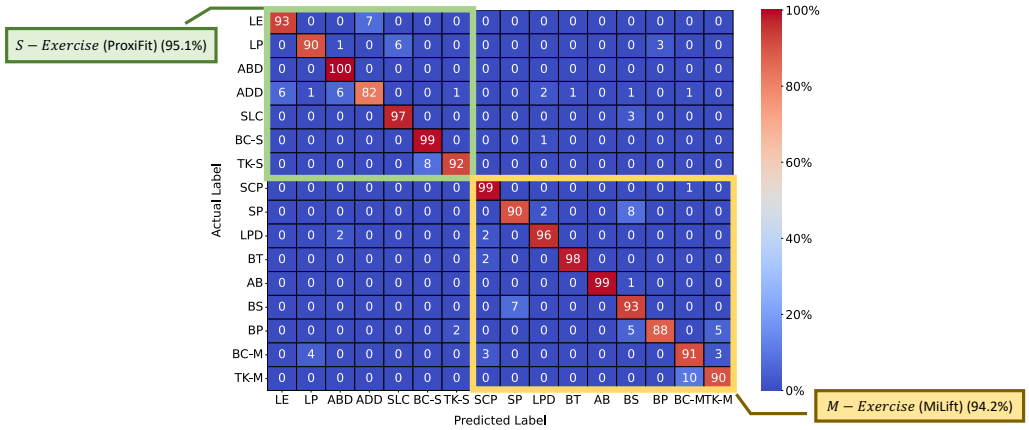

Fig. 14. Confusion matrix of end-to-end exercise classifications along natural gym routines (avg. 93.1%)

Figure 14 shows the end-to-end classification results on 11.6 hours of data. The average counting error is 0.77 reps per 10-rep session, which is even better than the 1.22 reps error seen in §7. Our supplemental video demonstrates a user's continuous gym routine where ProxiFit seamlessly determines workouts and non-workouts, classifies the right exercise type, and counts the repetitions in real-time, without any user intervention along the entire gym routine.

9.2 Signage Mode Performances

As pitched in §1, we newly present the signage mode – placing the sensing smartphone at an off-body, line-of-sight location so that the user can watch the visual contents while the proximity magnetic sensing monitors the exercise.

We evaluate the signage mode in all 3 categories. Figure 5 shows how the phone was mounted at each exercise. For lower-body & upper-body machines, the phone is gripped by a holder anchored to the machine. For free-weights, the phone holder is anchored to a separate stand. We let each user freely adjust the phone's position so that they can view the screen comfortably while lifting weights. If commercially deployed, the machine manufacturer or the gym owner could affix a permanent holder at a convenient location. We want to emphasize that this is a likely assumption reflecting the real market, considering the high demand for smartphone holders for gym use [10, 15], as explained in §1.

$\mathcal{D}_4$ in Table 2 is collected from the signage mode. With 9 users and the single-person training, Figure 15 shows the average classification results, which are perfect except for single-arm free weights. The average counting error is 0.69 rep per 10-rep session. In signage mode, single-arm free-weights are always $\mathcal{S}$-*Exercise*s regardless of sidedness. Thus, distinguishing the arm's sidedness is more challenging, as Figure 15a show on BC-L, BC-R, TK-L, TK-R. (-L & -R denote left & right arm, respectively.) If we consider sidedness-agnostic signage, Figure 15b shows perfect classification.

We verify that signage mode is highly reliable across many popular exercise types covering most categories of weight exercises. Having signage as an underlying sensing layer, rich visual interfaces (e.g., a virtual coach or video player) could be built upon it, opening unique interactions to the COTS device-based pervasive weight exercise tracking.

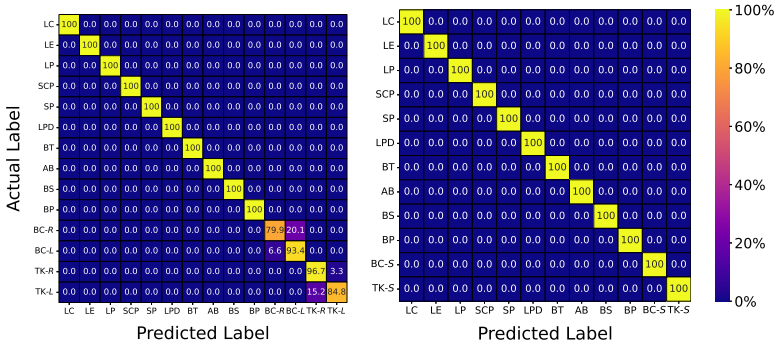

(a) Left- & right-arm free-weights separated (97.7%) (b) Agnostic to free-weight sideness (100%)

Fig. 15. Confusion matrices of signage mode exercise classification

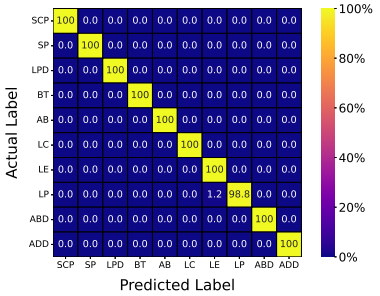

Fig. 16. Confusion matrix of exercise classification on Apple Watch (average 99.9%)

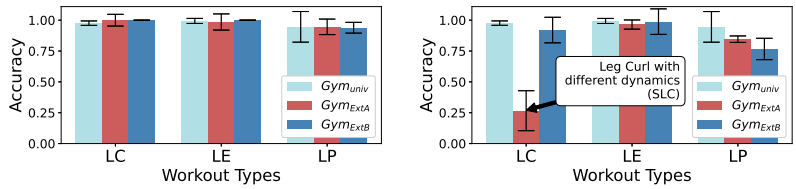

(a) Unmodified architecture and hyperparameters; retrained model (b) Unmodified model, architecture, and hyperparameters

Fig. 17. Portability of ProxiFit across gyms, tested under two different training conditions.

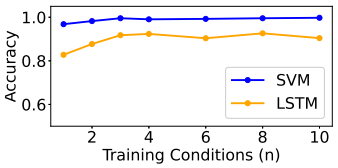

Fig. 18. Incremental learning effects of SVM and LSTM classifiers

9.3 Wearable Mode with a Watch

To verify iPhone is a good representative of Apple Watch, we have ProxiFit single-person-trained from $\mathcal{D}_1$ (collected from an iPhone), and test them onto $\mathcal{D}_5$ and $\mathcal{D}_6$ collected from an Apple Watch. Figure 16 showcases the accuracy for 5 lower- and 5 upper-body weight machines. SCP, SP, LPD, BT, and AB are upper-body weight machines (full names in Figure 4) and thereby $\mathcal{M}$-*Exercises* for a watch worn on the wrist. These are supported by incorporating $\mathcal{M}$-ProxiFit explained in §10. They demonstrate that our system is usable with either device interchangeably, not specifically biased to the phone. We clarify that $\mathcal{D}_5$ and $\mathcal{D}_6$ are inevitably small due to Apple's proprietary preemption policy hampering continuous sensing over a long period on an Apple Watch, as discussed in §3.2 and §8.

9.4 Portability to Other Gyms

Most experiments so far have been done at our university gym, Gym_{univ}. Now we extend to different gyms – Gym_{ExtA} and Gym_{ExtB}. We examine ProxiFit's across-gym portability under two different conditions.

9.4.1 Unmodified architecture & hyperparameters but retrained model. Firstly, we deploy the unmodified ProxiFit architecture and hyperparameters (i.e., window size and overlap) to different gyms. But we retrain the classifier for the new gym, under the single-person training policy. ProxiFit loads the gym-specific model at runtime, by applying a PoI-level localization technique [74, 75, 85]. This is our default premise of how to deploy ProxiFit at an unseen gym on Day 1. Although $\mathcal{D}_1$ from Gym_{univ} that granted us exclusive slots for experiments, Gym_{ExtA}

Table 4. Classification results between neighboring machines (Eleven sessions per each combination)

Machine in use		Machine where classification is done	
Leg Curl	Leg Extension	Leg Curl	Leg Extension
Active	Idle	*Leg Curl*	**Not detected**
Idle	Active	**Not detected**	*Leg Extension*
Active	Active	*Leg Curl*	*Leg Extension*

and Gym_{ExtB} did not – they were open to the public and machines were occupied most time. So, $\mathcal{D}_2$ and $\mathcal{D}_3$ are smaller. Moreover, these gyms are more challenging to ProxiFit as they are crowded, and thus inter-machine interference is pervasive.

Figure 17a shows the average accuracy of 97.6% and 98.0% after deploying the system and hyperparameters as-is, while retraining the model, to Gym_{ExtA} and Gym_{ExtB}, respectively. The original accuracy at Gym_{univ} was 97.2%. The repetition counter reports an average error of 0.48 and 0.84 rep per 10-rep session, from a total of 566 sessions. These results verify that ProxiFit is portable to unseen gyms and machines without changing its logic or hyperparameters.

9.4.2 Unmodified architecture & hyperparameters & model. Next, we explore beyond our default premise. We deploy everything unmodified to different gyms, without retraining the classifiers. The literature of soft-iron distortions and spontaneous magnetization in §2.5 teaches that, in theory, a model trained for specific weight machine instances is not directly portable to another gym; same-type machine pairs between two gyms are still different instances.

The leg press and leg extension of the three gyms share the same mechanical dynamics despite different brands. By applying a model pre-trained for Gym_{univ} as-is to Gym_{ExtA} and Gym_{ExtB}, Figure 17b shows a modest accuracy drop of 0.6%p-17.9%p for each same-type machine, except a 71%p drop for the seated leg curl (SLC) in Gym_{ExtA}. This excessive drop is due to SLC's large structural difference from the lying leg curl (LC) (in Gym_{univ} and Gym_{ExtB}), as seen in Figure 3(a) and (b). The takeaways from these experiments are: (1) Models perform best when trained per instance & per gym. (2) Yet the trained model is partially portable to a same-type machine at another gym, at a modest accuracy drop as long as the machine is of a similar structure. (3) This observation sheds light on the graceful bootstrapping of a newly brought machine or equipment, where its own instance-specific training is not immediately doable.

9.5 Effectiveness of Incremental Learning

So far, we focused on bootstrapping ProxiFit in a brand-new gym under single-person training constraint. Once bootstrapped, unlabeled data will accumulate as many users exercise with ProxiFit. We test semi-supervised learning to incrementally improve the model on-the-fly. Specifically, we take new exercise samples conditionally with a confidence threshold on the predictions from single-person trained SVM. Then we train both SVM and LSTM by one iteration using the predicted labels presumed to be true. Figure 18 depicts the incremental growth of both models along with newly incoming users, followed by a plateau. The results are averaged over multiple permutations of the ordering of incoming users. The data-hungry LSTM starts lower. As new users come in, LSTM's accuracy grows faster, narrowing the accuracy gap to the SVM. Still, a 'crossover' did not happen; rather the plateaus are formed before closing the gap.

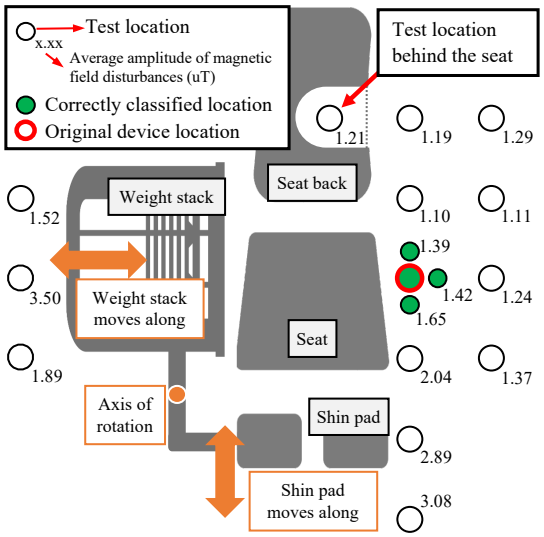

Fig. 19. Classification results and average amplitude of magnetic field disturbances (uT) observed around the leg extension machine for ten 10-repetition sets.

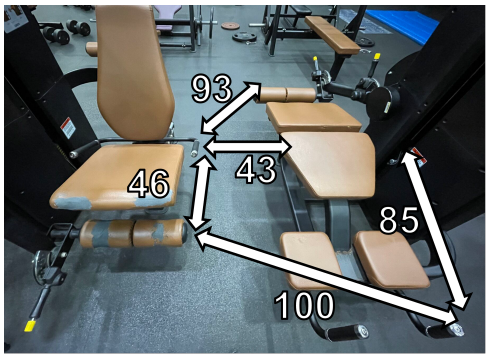

Fig. 20. Distance between closest neighboring machines, as close as 43 cm

9.6 Robustness of ProxiFit

9.6.1 Magnetic interference between adjacent machines. In a real gym, many people exercise simultaneously. One may worry about magnetic interference when neighboring machines are in use [85, 86]. We tested with two users exercising on adjacent machines, as shown in Figure 20. For space-saving, we detail a particular pair of machines – leg extension (LE) and leg curl (LC). This pair is chosen for showcasing because their inter-machine spacing is the shortest (43 cm) out of all adjacent machines in our gym, and thereby their inter-machine interference should be the strongest. Note that this spacing is even smaller than the legal minimum–at least 76.2 × 121.92 cm for wheelchair clearance [14].

Eleven sessions per each simultaneous exercise combination in both wearable and signage modes, we still observed no erroneous classification. Figure 4 summarizes experiment setups and results. In short, remote interference did not hinder local exercise detection, and there was no false-positive even if the user is holding the handle steadily without exercise.

To explain the anti-interference robustness showcased above, we point out that our PCA-driven features reflect the device's specific location and posture upon the user correctly gripping the handle of the target machine. *Simply being close enough to a machine does not necessarily produce a false-positive label.* To re-confirm this claim, we profiled the surrounding area around the leg extension machine for ten 10-repetition sets per each location. Figure 19 demonstrates simplified diagram of leg extension, the sampled locations, average amplitude of magnetic field disturbances at given locations, and classification results. Note that the sampled locations are of various distances to the moving metallic structure of the machine, and thereby observe various magnetic intensities when exercising, as annotated in Figure 19. The device's orientation and z-height above the ground are kept the same as the case at the handle. The results are promising. Only the locations close enough to the legitimate location (the handle) produce correct classifications; the classifier does not produce false-positive labels at other locations, including those closer to the machine and/or observing stronger magnetic disturbances. Overall, ProxiFit exhibits robustness from interference even between machines abnormally close below the regulated minimum.

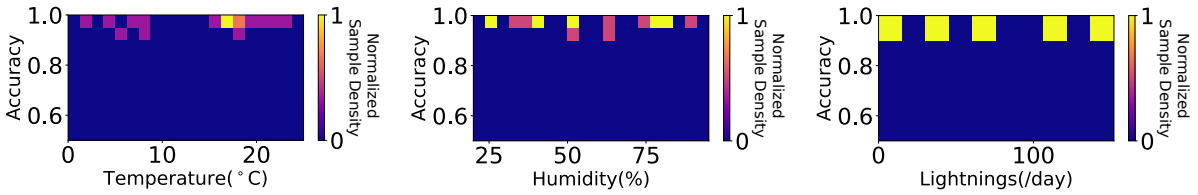

(a) Temperature (°C) (b) Humidity (%) (c) Lightnings (/day)

Fig. 21. Sample density maps showing robustness against varying weather conditions

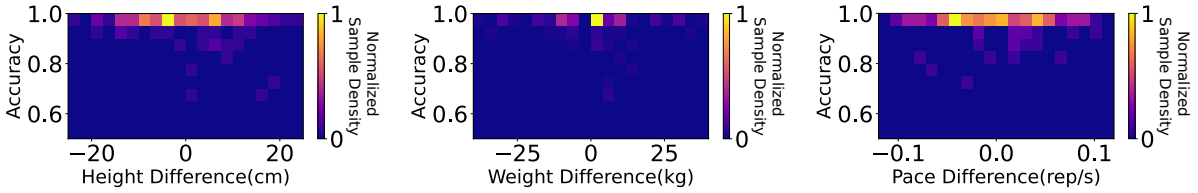

(a) Difference in user height (cm) (b) Difference in lifting weight (kg) (c) Difference in repetition pace

Fig. 22. Sample density maps showing robustness against various user physiques and exercise paces

9.6.2 Long-term aging of intrinsic magnetism. To suppress the operational cost, the once-trained magnetic patterns should remain valid as long as possible. To evaluate ProxiFit's possible 'aging' effects, we sampled two dates from $\mathcal{D}_1$: one on Aug. 22, 2021, and the other on Feb. 27, 2022. We trained a model with a single person's data in the former and tested it on different users' data in the latter. Repeating over 8 distinct single-person trained models gives an average of 97.1% accuracy. This result supports the longitudinal stability of the magnetic signature, for at least a 6-month span.

9.6.3 Robustness against weather-borne variations. It is known that weather factors may influence ambient magnetic fields [52]. We backtracked the past weather on the dates of data collection. Figure 21a through 21c show the density plots of the accuracy along the range of weather conditions–temperature, humidity, and number of lightning per day, respectively, at the time of experiments. Figure 21c has few samples as lightning struck on few days. In all weather variables, most samples exhibit near-top accuracies; no significant influence on the accuracy is observed.

9.6.4 Robustness against user-dependent variations. Figure 22a through 22c show the density plots of the accuracy along the users' body height, favorite lifting weight, and favorite repetition pace, respectively. For example, the x-axis of Figure 22a represents the body height differences between the (single-person) trained user and the tested users. In all variables, most samples exhibit near-top accuracies. Note that the samples may look skewed as we let the users freely choose a favorite weight and pace. The uneven x-axis distribution in Figure 22b and 22c reflect their natural choices.

9.6.5 Robustness against spatial displacement. For free-weight exercises in signage mode, recall §9.2 that the users freely positioned the phone along the horizontal (H), vertical (V), and distance (D) axes, for comfortable viewing. We found that the user-positioned phone locations fall in a 3-D box of $H \times V \times D = 20 \times 20 \times 20$ cm^3. Given this observation, we mimic the phone's likely displacements to six off-center positions, as shown in Figure 23a along with the resulting accuracy. We assess that ProxiFit is robust within the range enclosing the user-chosen displacements observed in §9.2.

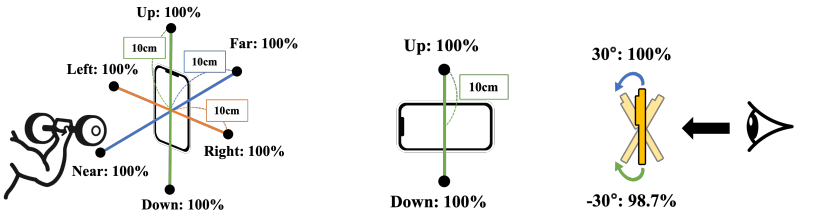

(a) Displaced to 6 positions during free-weight exercise (avg. accuracy 100%)

(b) Displaced to 2 positions during machine exercise (avg. accuracy 100%)

(c) Tilted to 2 orientations during machine exercise (average accuracy 99.4%)

Fig. 23. Signage mode robustness against phone displacement or tilt

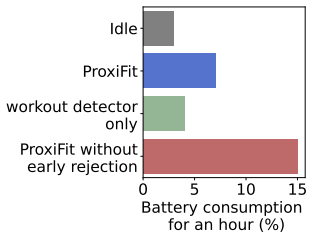

Fig. 24. Battery consumption on Apple Watch (for 1 hour)

Table 5. Biceps-curl classification: accuracy remains unaffected even with dumbbells changed.

Dumbbell	d_1	d_2	d_3
Wearable mode accuracy (%)	100	100	100
Signage mode accuracy (%)	100	100	100

In case of signage mode, users may slightly adjust the phone holder for individually best viewing experiences. We displaced the phone vertically by [+10, -10] cm and tilted by [+30°, -30°] range as illustrated in Figure 23b. Vertical displacement is fundamentally identical to Figure 23a, reproducing the same robust results. However, tilting smartphones renders the ambient magnetic field vectors to be largely rotated. Our signage mode omitted the frame normalizer as we assumed a fixed phone holder. Now relaxing the assumption and enabling again the frame normalizer to signage, ProxiFit achieved an average accuracy of 99.4% under the tilt over [+30°, -30°] range, as shown in Figure 23c.

9.6.6 Different dumbbells in free-weight. Unlike machine exercises, free-weights are not bound to a specific weight instance. Would ProxiFit keep stable classification with different dumbbells whose spontaneous magnetism may differ? We trained the classifier for a dumbbell d_0 and tested it upon 3 different dumbbells: d_1, d_2, d_3. Table 5 list the accuracy when the users performed biceps curl in the wearable mode and in the signage mode, respectively. Each mode employed a full-fledged classifier that classifies every exercise of the $\mathcal{S}$-*Exercise* family in the respective mode.

9.7 Power Consumption of System

ProxiFit is designed to run in the background throughout a user's gym routine; a gym routine may last for 1-2 hours, and thus the runtime battery consumption matters. To run autonomously free of user intervention, the workout detector runs for the entire gym routine, selectively triggering the exercise classifier and the repetition counter upon detection. It is reported that real-usage traces are crucial to fairly assess the battery consumption of continuous background sensing services [70, 94–97]. We measure the battery consumption along a 1-hour natural gym routine which contains a total of 25 minutes of net exercise time.

Figure 24 shows that ProxiFit drained the Apple Watch's battery only by 7%, compared to 3% drop at idle. This is attributable to the lightweight early rejection. To verify this, we run two ablations for an hour where one only runs sensor data collection and early rejection (i.e. no classification or repetition counting) and the other runs the entire pipeline all the time (i.e. no early rejection). The result shows early rejection drained the battery by 4%,

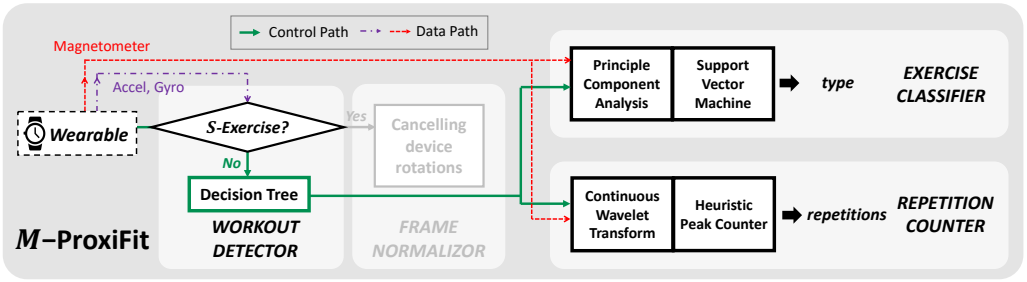

Fig. 25. $\mathcal{M}$-ProxiFit architecture, which is a trimmed-down version of the original ProxiFit architecture.

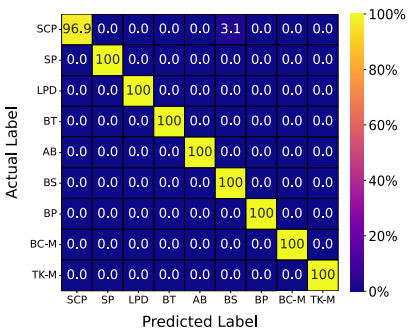

Fig. 26. $\mathcal{M}$-ProxiFit $\mathcal{M}$-*Exercise* classifications (99.7%)

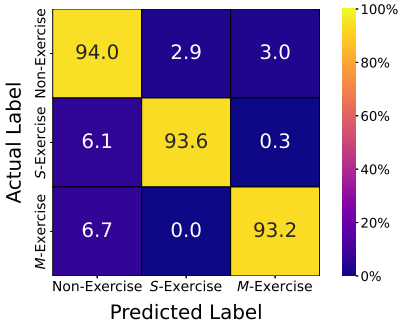

Fig. 27. $\mathcal{M}$-ProxiFit workout detection (93.8%)

which is only 1% more than being idle. On the other hand, running the whole pipeline without early rejection consumed 15% battery.

10 $\mathcal{M}$-PROXIFIT: EXTENDING PROXIFIT TO $\mathcal{S}$-*EXERCISES*

Until now, we mainly focused on new possibilities, i.e., $\mathcal{S}$-*Exercises*, that ProxiFit can bring by proximity sensing. But ProxiFit is not limited to stationary-device scenarios. In principle, magnetometer readings can change if either (a) the surrounding magnetic field changes, (b) the sensor itself travels through varying environmental fields, or (c) both (a) and (b). Obviously, $\mathcal{S}$-*Exercises* correspond to the case of (a), while $\mathcal{M}$-*Exercises* correspond to (b) or (c).

To explore the latter potential of sensing $\mathcal{M}$-*Exercises* magnetically instead of using traditional IMUs, we developed $\mathcal{M}$-ProxiFit, a minor variant of ProxiFit retrofitted for $\mathcal{M}$-*Exercises*, which co-exists with the original ProxiFit and replaces the role of MiLift taking care of processing $\mathcal{M}$-*Exercises*. Figure 25 shows the architecture of $\mathcal{M}$-ProxiFit. The changes from the original ProxiFit are mainly two-fold. First, the frame normalizer is omitted to preserve rotational information. Second, the workout detector is replaced with a simple decision tree based on autocorrelation and power.

We test a new implementation where ProxiFit detects $\mathcal{S}$-*Exercises* and $\mathcal{M}$-ProxiFit detects $\mathcal{M}$-*Exercises*. Figure 26 presents its accuracy (99.7%) tested on $\mathcal{D}_1$, which outperforms IMU-based MiLift (94.2%) seen in Figure 14. Segmentation performance is also shown in Figure 27. Figure 28 visualizes segmentation results of along continuous gym routines. For repetition counting, evaluation on $\mathcal{M}$-*Exercises* in $\mathcal{D}_1$ reports an average error of 0.38 rep per 10-rep session.

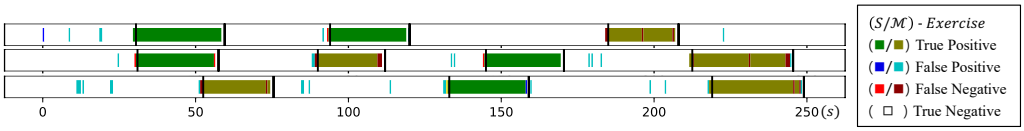

Fig. 28. Detailed view of detected segments by $\mathcal{M}$-ProxiFit along a part of continuous gym routine

11 DISCUSSION

Augmentation using magnets. Inspired from magnetic instrumentation [26, 33, 61], ProxiFit may augment a machine's natural magnetism by attaching a small magnet, preferably on a moving part quite far away from the user. It may, however, bring the side-effect of increased interference to nearby machines.

Miscellaneous clarifications. While most weight machines come with a built-in weight stack, a few machines such as the leg press (LP) in $\mathcal{D}_1$ accept external weight discs whose magnetic signature would be diverse. Fortunately, our experiments support that their magnetic disturbance patterns are rather stable. We believe that the machine's moving frame (where discs are hung; much heavier than the discs) dominates the total weight disturbances.

Malicious magnetic attack. Ferromagnetic materials has remanence – a residual magnetism after exposure to an extreme external magnetic field (e.g., 1.0 T) [28]. Although it is an MRI-grade strength, some experimental magnets are so strong; a malicious user might bring one to alter a machine's magnetic pattern, yet it is unlikely in practice.

12 CONCLUSION

We presented ProxiFit, a novel proximity magnetic monitoring system supporting most weight exercise categories frequently performed at gyms: lower-body machines, upper-body machines, and free-weight. ProxiFit leverages the intrinsic magnetism of weight equipment. ProxiFit uses only a single commodity mobile device that most users already own, i.e., either a smartphone or a smartwatch, and does not require any instrumentation on the equipment or the gym space. ProxiFit brings two unprecedented features to commodity COTS device-based weight exercise tracking: (1) its wearable mode newly supports previously unsupported weight exercise categories while ensuring the natural way to wear that device; (2) it features the new signage mode, enabling rich user-device visual interaction while the exercises are being tracked in the background. We developed a prototype of ProxiFit on iPhone 12 Pro and Apple Watch Series 6. We addressed the unique signals and learning challenges, and verified its performance and usability along with natural end-to-end gym routines as well as against diverse reality factors expected in real, longitudinal deployment.

ACKNOWLEDGMENTS

This work was partly supported by Institute of Information & communications Technology Planning & Evaluation (IITP) grant funded by the Korea government(MSIT) (No.2019-0-01906, Artificial Intelligence Graduate School Program(POSTECH)) and Basic Science Research Program through the National Research Foundation of Korea(NRF) funded by the Ministry of Education(2022R1A6A1A03052954). This research was also partly supported by the National Research Foundation of Korea(NRF) grant funded by the Korea government(MSIT) (No. 2021R1A2C200386612), by the IITP grants by the MSIT, Korea (IITP-2020-0-01778), and by the Alchemist Project NTIS1415187366(20025752) funded by the Ministry of Trade, Industry & Energy(MOTIE, Korea).

REFERENCES

[1] 2018. Wearable Tech is New Top Fitness Trend for 2019, (American College of Sports Medicine). Retrieved Feb. 9, 2023 from https://www.acsm.org/old-pages/news-releases/news-detail/2018/12/05/wearable-tech-top-2019-fitness-trend

[2] 2019. Wearable Tech Named Top Fitness Trend for 2020 (American College of Sports Medicine). Retrieved Feb. 9, 2023 from https://www.acsm.org/old-pages/news-releases/news-detail/2019/10/30/wearable-tech-named-top-fitness-trend-for-2020
[3] 2020. Apple Watch Series 6 Teardown (iFixit). Retrieved May. 14, 2023 from https://www.ifixit.com/Teardown/Apple+Watch+Series+6+Teardown/136694#s271741
[4] 2020. iPhone 12 and 12 Pro Teardown (iFixit). Retrieved May. 14, 2023 from https://www.ifixit.com/Teardown/iPhone+12+and+12+Pro+Teardown/137669#s274761
[5] 2021. iPhone 13 Pro Full Chip ID. Retrieved May. 15, 2023 from https://www.ifixit.com/Guide/iPhone+13+Pro+Full+Chip+ID/144993#s294054
[6] 2021. Wearable Tech Named Top Fitness Trend for 2022 (American College of Sports Medicine). Retrieved Feb. 9, 2023 from https://www.acsm.org/news-detail/2021/12/30/wearable-tech-named-top-fitness-trend-for-2022
[7] 2022. Wearable Technology Named Top Fitness Trend for 2023 (American College of Sports Medicine). Retrieved Feb. 9, 2023 from https://www.acsm.org/news-detail/2022/12/28/wearable-technology-named-top-fitness-trend-for-2023
[8] 2023. AIToolbox (Kevin Coble). Retrieved Feb. 9, 2023 from https://github.com/KevinCoble/AIToolbox
[9] 2023. ALPS Geomagnetic Sensors. Retrieved May. 15, 2023 from https://tech.alpsalpine.com/e/products/category/sensor/sub/02/
[10] 2023. Belkin Fitness Mount. Retrieved May. 13, 2023 from https://www.amazon.com/Belkin-compatible-Equipment-Cellphone-Elliptical/dp/B091LBM27P
[11] 2023. COROS. Retrieved Feb. 9, 2023 from https://www.coros.com
[12] 2023. Garmin. Retrieved Feb. 9, 2023 from https://www.garmin.com
[13] 2023. Geomagnetic Type HSCD Series. Retrieved May. 15, 2023 from https://tech.alpsalpine.com/e/products/category/sensor/sub/02/series/hscd/
[14] 2023. Guide to the ABA: Sports Facilities (U.S. Access Board). Retrieved Feb. 9, 2023 from https://www.access-board.gov/aba/guides/chapter-10-sports-facilities/
[15] 2023. Gym Buddy gym mount. Retrieved May. 15, 2023 from https://www.amazon.com/Magnetic-Phone-Holder-Stick-Metal/dp/B07J2Y4DNG
[16] 2023. Gymatic Workout Tracker. Retrieved Feb. 9, 2023 from https://apps.apple.com/us/app/gymatic-workout-tracker/id1036069872
[17] 2023. Running Workout Sessions: Track a workout on Apple Watch. Retrieved Feb. 9, 2023 from https://developer.apple.com/documentation/healthkit/workouts_and_activity_rings/running_workout_sessions
[18] 2023. Speediance Home Gym. Retrieved May. 13, 2023 from https://www.speediance.com/products/speediance-home-gym
[19] 2023. wavelib (Rafat Hussain). Retrieved Feb. 9, 2023 from https://github.com/rafat/wavelib
[20] Miru Ahn, Sungjun Kwon, Byunglim Park, Kyungmin Cho, Sungwon Peter Choe, Inseok Hwang, Hyukjae Jang, Jaesang Park, Yunseok Rhee, and Junehwa Song. 2009. Running or gaming. In *Proceedings of the international conference on advances in computer entertainment technology*. 345–348.
[21] Aino Ahtinen, Elina Mattila, Antti Vaatanen, Lotta Hynninen, Jukka Salminen, Esa Koskinen, and Klaus Laine. 2009. User experiences of mobile wellness applications in health promotion: User study of Wellness Diary, Mobile Coach and SelfRelax. In *2009 3rd International Conference on Pervasive Computing Technologies for Healthcare*. 1–8. https://doi.org/10.4108/ICST.PERVASIVEHEALTH2009.6007
[22] Stephanie Alley, Stephanie Schoeppe, Diana Guertler, Cally Jennings, Mitch J Duncan, and Corneel Vandelanotte. 2016. Interest and preferences for using advanced physical activity tracking devices: results of a national cross-sectional survey. *BMJ open* 6, 7 (2016), 011243.
[23] Swamy Ananthanarayan, Miranda Sheh, Alice Chien, Halley Profita, and Katie Siek. 2013. Pt Viz: towards a wearable device for visualizing knee rehabilitation exercises. In *Proceedings of the SIGCHI Conference on Human Factors in Computing Systems*. 1247–1250.
[24] James J. Annesi. 2001. Effects of music, television, and a combination entertainment system on distraction, exercise adherence, and physical output in adults. *Canadian Journal of Behavioural Science* 33 (2001), 193–202.
[25] Paramasiven Appavoo, Mun Choon Chan, and Anand Bhojan. 2020. MagB: Repurposing the Magnetometer for Fine-Grained Localization of IoT Devices. In *IEEE INFOCOM 2020-IEEE Conference on Computer Communications*. IEEE, 2391–2399.
[26] Daniel Ashbrook, Patrick Baudisch, and Sean White. 2011. Nenya: subtle and eyes-free mobile input with a magnetically-tracked finger ring. In *Proceedings of the SIGCHI Conference on Human Factors in Computing Systems*. 2043–2046.
[27] Neil W Ashcroft, N David Mermin, et al. 1976. Solid state physics.
[28] SK Banerjee and JP Mellema. 1974. A new method for the determination of paleointensity from the ARM properties of rocks. *Earth and Planetary Science Letters* 23, 2 (1974), 177–184.
[29] Sizhen Bian, Vitor F Rey, Peter Hevesi, and Paul Lukowicz. 2019. Passive capacitive based approach for full body gym workout recognition and counting. In *2019 IEEE International Conference on Pervasive Computing and Communications (PerCom*. IEEE, 1–10.
[30] Meghan L Butryn, Danielle Arigo, Greer A Raggio, Marie Colasanti, and Evan M Forman. 2016. Enhancing physical activity promotion in midlife women with technology-based self-monitoring and social connectivity: a pilot study. *Journal of health psychology* 21, 8 (2016), 1548–1555.

[31] Chih-Chung Chang and Chih-Jen Lin. 2011. LIBSVM: a library for support vector machines. *ACM transactions on intelligent systems and technology (TIST)* 2, 3 (2011), 1–27.

[32] Keng-hao Chang, Mike Y Chen, and John Canny. 2007. Tracking free-weight exercises. In *International Conference on Ubiquitous Computing*. Springer, 19–37.

[33] Dongyao Chen, Mingke Wang, Chenxi He, Qing Luo, Yasha Iravantchi, Alanson Sample, Kang G Shin, and Xinbing Wang. 2021. MagX: wearable, untethered hands tracking with passive magnets. In *Proceedings of the 27th Annual International Conference on Mobile Computing and Networking*. 269–282.

[34] Ke-Yu Chen, Kent Lyons, Sean White, and Shwetak Patel. 2013. uTrack: 3D input using two magnetic sensors. In *Proceedings of the 26th annual ACM symposium on User interface software and technology*. 237–244.

[35] Ke-Yu Chen, Shwetak N Patel, and Sean Keller. 2016. Finexus: Tracking precise motions of multiple fingertips using magnetic sensing. In *Proceedings of the 2016 CHI Conference on Human Factors in Computing Systems*. 1504–1514.

[36] Ke-Yu Chen, Rahul C. Shah, Jonathan Huang, and Lama Nachman. 2017. Mago: Mode of Transport Inference Using the Hall-Effect Magnetic Sensor and Accelerometer. *Proc. ACM Interact. Mob. Wearable Ubiquitous Technol.* 1, 2, Article 8 (jun 2017), 23 pages. https://doi.org/10.1145/3090054

[37] Yushi Cheng, Xiaoyu Ji, Wenyuan Xu, Hao Pan, Zhuangdi Zhu, Chuang-Wen You, Yi-Chao Chen, and Lili Qiu. 2019. MagAttack: Guessing application launching and operation via smartphone. In *Proceedings of the 2019 ACM Asia Conference on Computer and Communications Security*. 283–294.

[38] Soshin Chikazumi and Chad D Graham. 2009. *Physics of Ferromagnetism 2e*. Number 94. Oxford University Press on Demand. 118–124 pages.

[39] Sungjae Cho, Yoonsu Kim, Jaewoong Jang, and Inseok Hwang. 2023. AI-to-Human Actuation: Boosting Unmodified AI's Robustness by Proactively Inducing Favorable Human Sensing Conditions. *Proceedings of the ACM on Interactive, Mobile, Wearable and Ubiquitous Technologies* 7, 1 (2023), 1–32.

[40] Woohyeok Choi, Jeungmin Oh, Taiwoo Park, Seongjun Kang, Miri Moon, Uichin Lee, Inseok Hwang, Darren Edge, and Junehwa Song. 2016. Designing interactive multiswimmer exergames: a case study. *ACM Transactions on Sensor Networks (TOSN)* 12, 3 (2016), 1–40.

[41] Woohyeok Choi, Jeungmin Oh, Taiwoo Park, Seongjun Kang, Miri Moon, Uichin Lee, Inseok Hwang, and Junehwa Song. 2014. MobyDick: an interactive multi-swimmer exergame. In *Proceedings of the 12th ACM Conference on Embedded Network Sensor Systems*. 76–90.

[42] Jaewoo Chung, Matt Donahoe, Chris Schmandt, Ig-Jae Kim, Pedram Razavai, and Micaela Wiseman. 2011. Indoor location sensing using geo-magnetism. In *Proceedings of the 9th international conference on Mobile systems, applications, and services*. 141–154.

[43] Caleb Conner and Gene Michael Poor. 2016. Correcting exercise form using body tracking. In *Proceedings of the 2016 CHI Conference Extended Abstracts on Human Factors in Computing Systems*. 3028–3034.

[44] C Crema, A Depari, A Flammini, Emiliano Sisinni, T Haslwanter, and S Salzmann. 2017. IMU-based solution for automatic detection and classification of exercises in the fitness scenario. In *2017 IEEE Sensors Applications Symposium (SAS)*. IEEE, 1–6.

[45] Bernard Dennis Cullity and Chad D Graham. 2011. *Introduction to magnetic materials*. John Wiley & Sons.

[46] Cybex. 2023. YouTube Channel. Retrieved May. 13, 2023 from https://www.youtube.com/@Cybexintl

[47] Han Ding, Longfei Shangguan, Zheng Yang, Jinsong Han, Zimu Zhou, Panlong Yang, Wei Xi, and Jizhong Zhao. 2015. Femo: A platform for free-weight exercise monitoring with rfids. In *Proceedings of the 13th ACM Conference on Embedded Networked Sensor Systems*. 141–154.

[48] Moustafa Elhamshary, Moustafa Youssef, Akira Uchiyama, Hirozumi Yamaguchi, and Teruo Higashino. 2016. TransitLabel: A crowd-sensing system for automatic labeling of transit stations semantics. In *Proceedings of the 14th annual international conference on mobile systems, applications, and services*. 193–206.

[49] Xirui Fan, Jing Wu, Chengnian Long, and Yanmin Zhu. 2017. Accurate and low-cost mobile indoor localization with 2-D magnetic fingerprints. In *Proceedings of the First ACM Workshop on Mobile Crowdsensing Systems and Applications*. 13–18.

[50] Bruno Ferreira, Pedro M Ferreira, Gil Pinheiro, Nelson Figueiredo, Filipe Carvalho, Paulo Menezes, and Jorge Batista. 2021. Deep learning approaches for workout repetition counting and validation. *Pattern Recognition Letters* 151 (2021), 259–266.

[51] Life Fitness. 2023. YouTube Channel. Retrieved May. 13, 2023 from https://www.youtube.com/@lifefitness

[52] AC Fraser-Smith. 1993. ULF magnetic fields generated by electrical storms and their significance to geomagnetic pulsation generation. *Geophysical research letters* 20, 6 (1993), 467–470.

[53] Thomas Fritz, Elaine M Huang, Gail C Murphy, and Thomas Zimmermann. 2014. Persuasive technology in the real world: a study of long-term use of activity sensing devices for fitness. In *Proceedings of the SIGCHI conference on human factors in computing systems*. 487–496.

[54] Biying Fu, Dinesh Vaithyalingam Gangatharan, Arjan Kuijper, Florian Kirchbuchner, and Andreas Braun. 2017. Exercise monitoring on consumer smart phones using ultrasonic sensing. In *Proceedings of the 4th international Workshop on Sensor-based Activity Recognition and Interaction*. 1–6.

[55] Biying Fu, Florian Kirchbuchner, and Arjan Kuijper. 2020. Unconstrained workout activity recognition on unmodified commercial off-the-shelf smartphones. In *Proceedings of the 13th ACM International Conference on PErvasive Technologies Related to Assistive Environments*. 1–10.

[56] Xiaonan Guo, Jian Liu, Cong Shi, Hongbo Liu, Yingying Chen, and Mooi Choo Chuah. 2018. Device-free personalized fitness assistant using WiFi. *Proceedings of the ACM on Interactive, Mobile, Wearable and Ubiquitous Technologies* 2, 4 (2018), 1–23.

[57] Nils Y Hammerla, Shane Halloran, and Thomas Plötz. 2016. Deep, convolutional, and recurrent models for human activity recognition using wearables. *arXiv preprint arXiv:1604.08880* (2016).

[58] Chris Harrison and Scott E Hudson. 2009. Abracadabra: wireless, high-precision, and unpowered finger input for very small mobile devices. In *Proceedings of the 22nd annual ACM symposium on User interface software and technology*. 121–124.

[59] Akpa Akpro Elder Hippocrate, Edith Talina Luhanga, Takata Masashi, Ko Watanabe, and Keiichi Yasumoto. 2017. Smart gyms need smart mirrors: design of a smart gym concept through contextual inquiry. In *Proceedings of the 2017 ACM International Joint Conference on Pervasive and Ubiquitous Computing and Proceedings of the 2017 ACM International Symposium on Wearable Computers*. 658–661.

[60] Bo-Jhang Ho, Renju Liu, Hsiao-Yun Tseng, and Mani Srivastava. 2017. Myobuddy: Detecting barbell weight using electromyogram sensors. In *Proceedings of the 1st Workshop on Digital Biomarkers*. 27–32.

[61] Hua Huang, Hongkai Chen, and Shan Lin. 2019. Magtrack: Enabling safe driving monitoring with wearable magnetics. In *Proceedings of the 17th Annual International Conference on Mobile Systems, Applications, and Services*. 326–339.

[62] Hua Huang and Shan Lin. 2020. MET: a magneto-inductive sensing based electric toothbrushing monitoring system. In *Proceedings of the 26th Annual International Conference on Mobile Computing and Networking*. 1–14.

[63] Inseok Hwang, Hyukjae Jang, Lama Nachman, and Junehwa Song. 2010. Exploring inter-child behavioral relativity in a shared social environment: a field study in a kindergarten. In *Proceedings of the 12th ACM international conference on Ubiquitous computing*. 271–280.

[64] Inseok Hwang, Hyukjae Jang, Taiwoo Park, Aram Choi, Youngki Lee, Chanyou Hwang, Yanggui Choi, Lama Nachman, and Junehwa Song. 2012. Leveraging children's behavioral distribution and singularities in new interactive environments: Study in kindergarten field trips. In *Pervasive Computing: 10th International Conference, Pervasive 2012, Newcastle, UK, June 18-22, 2012. Proceedings 10*. Springer, 39–56.

[65] Inseok Hwang, Youngki Lee, Taiwoo Park, and Junehwa Song. 2012. Toward a mobile platform for pervasive games. In *Proceedings of the first ACM international workshop on Mobile gaming*. 19–24.

[66] Inseok Hwang, Youngki Lee, Chungkuk Yoo, Chulhong Min, Dongsun Yim, and John Kim. 2019. Towards interpersonal assistants: next-generation conversational agents. *IEEE Pervasive Computing* 18, 2 (2019), 21–31.

[67] Inseok Hwang, Chungkuk Yoo, Chanyou Hwang, Dongsun Yim, Youngki Lee, Chulhong Min, John Kim, and Junehwa Song. 2014. TalkBetter: family-driven mobile intervention care for children with language delay. In *Proceedings of the 17th ACM conference on Computer supported cooperative work & social computing*. 1283–1296.

[68] Hyukjae Jang, Sungwon Peter Choe, Inseok Hwang, Chanyou Hwang, Lama Nachman, and Junehwa Song. 2012. RubberBand: augmenting teacher's awareness of spatially isolated children on kindergarten field trips. In *Proceedings of the 2012 ACM conference on ubiquitous computing*. 236–239.

[69] Bumsoo Kang, Inseok Hwang, Jinho Lee, Seungchul Lee, Taegyeong Lee, Youngjae Chang, and Min Kyung Lee. 2018. My being to your place, your being to my place: Co-present robotic avatars create illusion of living together. In *Proceedings of the 16th Annual International Conference on Mobile Systems, Applications, and Services*. 54–67.

[70] Bumsoo Kang, Chulhong Min, Wonjung Kim, Inseok Hwang, Chunjong Park, Seungchul Lee, Sung-Ju Lee, and Junehwa Song. 2017. Zaturi: We put together the 25th hour for you. create a book for your baby. In *Proceedings of the 2017 ACM Conference on Computer Supported Cooperative Work and Social Computing*. 1850–1863.

[71] Usman Ali Khan, Iftikhar Ahmed Khan, Ahmad Din, Waqas Jadoon, Rab Nawaz Jadoon, Muhammad Amir Khan, Fiaz Gul Khan, and Abdul Nasir Khan. 2020. Towards a Complete Set of Gym Exercises Detection Using Smartphone Sensors. *Scientific Programming* 2020 (2020), 1–12.

[72] Rushil Khurana, Karan Ahuja, Zac Yu, Jennifer Mankoff, Chris Harrison, and Mayank Goel. 2018. GymCam: Detecting, recognizing and tracking simultaneous exercises in unconstrained scenes. *Proceedings of the ACM on Interactive, Mobile, Wearable and Ubiquitous Technologies* 2, 4 (2018), 1–17.

[73] Rushil Khurana, Mayank Goel, and Kent Lyons. 2019. Detachable smartwatch: More than a wearable. *Proceedings of the ACM on Interactive, Mobile, Wearable and Ubiquitous Technologies* 3, 2 (2019), 1–14.

[74] Byoungjip Kim, SangJeong Lee, Youngki Lee, Inseok Hwang, Yunseok Rhee, and Junehwa Song. 2011. Mobiiscape: Middleware support for scalable mobility pattern monitoring of moving objects in a large-scale city. *Journal of Systems and Software* 84, 11 (2011), 1852–1870.

[75] Wonjung Kim, Seungchul Lee, Youngjae Chang, Taegyeong Lee, Inseok Hwang, and Junehwa Song. 2021. Hivemind: social control-and-use of IoT towards democratization of public spaces. In *Proceedings of the 19th Annual International Conference on Mobile Systems, Applications, and Services*. 467–482.

[76] Wonjung Kim, Seungchul Lee, Seonghoon Kim, Sungbin Jo, Chungkuk Yoo, Inseok Hwang, Seungwoo Kang, and Junehwa Song. 2020. Dyadic Mirror: Everyday Second-person Live-view for Empathetic Reflection upon Parent-child Interaction. *Proceedings of the ACM on*

Interactive, Mobile, Wearable and Ubiquitous Technologies 4, 3 (2020), 1–29.

[77] Yuhwan Kim, Seungchul Lee, Inseok Hwang, Hyunho Ro, Youngki Lee, Miri Moon, and Junehwa Song. 2014. High5: promoting interpersonal hand-to-hand touch for vibrant workplace with electrodermal sensor watches. In *Proceedings of the 2014 ACM International Joint Conference on Pervasive and Ubiquitous Computing*. 15–19.

[78] Gregory S Kolt, Grant M Schofield, Ngaire Kerse, Nicholas Garrett, Toni Ashton, and Asmita Patel. 2012. Healthy Steps trial: pedometer-based advice and physical activity for low-active older adults. *The Annals of Family Medicine* 10, 3 (2012), 206–212.

[79] Belal Korany and Yasamin Mostofi. 2021. Counting a stationary crowd using off-the-shelf wifi. In *Proceedings of the 19th Annual International Conference on Mobile Systems, Applications, and Services*. 202–214.

[80] Heli Koskimäki, Pekka Siirtola, and Juha Röning. 2017. Myogym: introducing an open gym data set for activity recognition collected using myo armband. In *Proceedings of the 2017 ACM International Joint Conference on Pervasive and Ubiquitous Computing and Proceedings of the 2017 ACM International Symposium on Wearable Computers*. 537–546.

[81] Haechan Lee, Miri Moon, Taiwoo Park, Inseok Hwang, Uichin Lee, and Junehwa Song. 2013. Dungeons & swimmers: designing an interactive exergame for swimming. In *Proceedings of the 2013 ACM conference on Pervasive and Ubiquitous Computing adjunct publication*. 287–290.

[82] Jinho Lee, Inseok Hwang, Thomas Hubregtsen, Anne E Gattiker, and Christopher M Durham. 2017. Sci-Fii: Speculative conversational interface framework for incremental inference on modularized services. In *2017 18th IEEE International Conference on Mobile Data Management (MDM)*. IEEE, 278–285.

[83] Jinho Lee, Inseok Hwang, Thomas S Hubregtsen, Anne E Gattiker, and Christopher M Durham. 2019. Accelerating conversational agents built with off-the-shelf modularized services. *IEEE Pervasive Computing* 18, 2 (2019), 47–57.

[84] Jungeun Lee, Sungnam Kim, Minki Cheon, Hyojin Ju, JaeEun Lee, and Inseok Hwang. 2022. SleepGuru: Personalized Sleep Planning System for Real-life Actionability and Negotiability. In *Proceedings of the 35th Annual ACM Symposium on User Interface Software and Technology*. 1–16.

[85] Youngki Lee, Younghyun Ju, Chulhong Min, Seungwoo Kang, Inseok Hwang, and Junehwa Song. 2012. Comon: Cooperative ambience monitoring platform with continuity and benefit awareness. In *Proceedings of the 10th international conference on Mobile systems, applications, and services*. 43–56.

[86] Youngki Lee, Seungwoo Kang, Chulhong Min, Younghyun Ju, Inseok Hwang, and Junehwa Song. 2015. CoMon+: A cooperative context monitoring system for multi-device personal sensing environments. *IEEE Transactions on Mobile Computing* 15, 8 (2015), 1908–1924.

[87] Xinye Lin, Yixin Chen, Xiao-Wen Chang, Xue Liu, and Xiaodong Wang. 2018. Show: Smart handwriting on watches. *Proceedings of the ACM on Interactive, Mobile, Wearable and Ubiquitous Technologies* 1, 4 (2018), 1–23.

[88] Yihao Liu, Kai Huang, Xingzhe Song, Boyuan Yang, and Wei Gao. 2020. Maghacker: eavesdropping on stylus pen writing via magnetic sensing from commodity mobile devices. In *Proceedings of the 18th International Conference on Mobile Systems, Applications, and Services*. 148–160.

[89] Chris Xiaoxuan Lu, Yang Li, Peijun Zhao, Changhao Chen, Linhai Xie, Hongkai Wen, Rui Tan, and Niki Trigoni. 2018. Simultaneous localization and mapping with power network electromagnetic field. In *Proceedings of the 24th annual international conference on mobile computing and networking*. 607–622.

[90] Kent Lyons. 2016. 2D input for virtual reality enclosures with magnetic field sensing. In *Proceedings of the 2016 ACM International Symposium on Wearable Computers*. 176–183.

[91] Kent Lyons. 2020. Wearable magnetic field sensing for finger tracking. In *Proceedings of the 2020 International Symposium on Wearable Computers*. 63–67.

[92] Nikolay Matyunin, Yujue Wang, Tolga Arul, Kristian Kullmann, Jakub Szefer, and Stefan Katzenbeisser. 2019. MagneticSpy: Exploiting Magnetometer in Mobile Devices for Website and Application Fingerprinting. In *Proceedings of the 18th ACM Workshop on Privacy in the Electronic Society* (London, United Kingdom) *(WPES'19)*. Association for Computing Machinery, New York, NY, USA, 135–149. https://doi.org/10.1145/3338498.3358650

[93] Jess McIntosh, Paul Strohmeier, Jarrod Knibbe, Sebastian Boring, and Kasper Hornbæk. 2019. Magnetips: Combining fingertip tracking and haptic feedback for around-device interaction. In *Proceedings of the 2019 CHI Conference on Human Factors in Computing Systems*. 1–12.

[94] Chulhong Min, Youngki Lee, Chungkuk Yoo, Inseok Hwang, Younghyun Ju, Junehwa Song, and Seungwoo Kang. 2019. Scalable Power Impact Prediction of Mobile Sensing Applications at Pre-Installation Time. *IEEE Transactions on Mobile Computing* 19, 6 (2019), 1448–1464.

[95] Chulhong Min, Youngki Lee, Chungkuk Yoo, Seungwoo Kang, Sangwon Choi, Pillsoon Park, Inseok Hwang, Younghyun Ju, Seungpyo Choi, and Junehwa Song. 2015. PowerForecaster: Predicting smartphone power impact of continuous sensing applications at pre-installation time. In *Proceedings of the 13th ACM Conference on Embedded Networked Sensor Systems*. 31–44.

[96] Chulhong Min, Youngki Lee, Chungkuk Yoo, Seungwoo Kang, Inseok Hwang, and Junehwa Song. 2016. PowerForecaster: Predicting power impact of mobile sensing applications at pre-installation time. *GetMobile: Mobile Computing and Communications* 20, 1 (2016), 30–33.

[97] Chulhong Min, Chungkuk Yoo, Inseok Hwang, Seungwoo Kang, Youngki Lee, Seungchul Lee, Pillsoon Park, Changhun Lee, Seungpyo Choi, and Junehwa Song. 2015. Sandra helps you learn: The more you walk, the more battery your phone drains. In *Proceedings of the 2015 ACM international joint conference on pervasive and ubiquitous computing*. 421–432.

[98] Frank Mokaya, Hae Young Noh, Roland Lucas, and Pei Zhang. 2018. MyoVibe: Enabling inertial sensor-based muscle activation detection in high-mobility exercise environments. *ACM Transactions on Sensor Networks (TOSN)* 14, 1 (2018), 1–26.

[99] Dan Morris, T Scott Saponas, Andrew Guillory, and Ilya Kelner. 2014. RecoFit: using a wearable sensor to find, recognize, and count repetitive exercises. In *Proceedings of the SIGCHI Conference on Human Factors in Computing Systems*. 3225–3234.

[100] Bobak Jack Mortazavi, Mohammad Pourhomayoun, Gabriel Alsheikh, Nabil Alshurafa, Sunghoon Ivan Lee, and Majid Sarrafzadeh. 2014. Determining the single best axis for exercise repetition recognition and counting on smartwatches. In *2014 11th international conference on wearable and implantable body sensor networks*. IEEE, 33–38.

[101] Robert C O'handley. 1999. *Modern magnetic materials: principles and applications*.

[102] Francisco Javier Ordóñez and Daniel Roggen. 2016. Deep convolutional and lstm recurrent neural networks for multimodal wearable activity recognition. *Sensors* 16, 1 (2016), 115.

[103] Martin A O'Reilly, Darragh F Whelan, Tomas E Ward, Eamonn Delahunt, and Brian Caulfield. 2017. Technology in strength and conditioning tracking lower-limb exercises with wearable sensors. *The Journal of Strength & Conditioning Research* 31, 6 (2017), 1726–1736.

[104] Hao Pan, Yi-Chao Chen, Guangtao Xue, and Xiaoyu Ji. 2017. Magnecomm: Magnetometer-based near-field communication. In *Proceedings of the 23rd Annual International Conference on Mobile Computing and Networking*. 167–179.

[105] Keunwoo Park, Daehwa Kim, Seongkook Heo, and Geehyuk Lee. 2020. MagTouch: Robust Finger Identification for a Smartwatch Using a Magnet Ring and a Built-in Magnetometer. In *Proceedings of the 2020 CHI Conference on Human Factors in Computing Systems*. 1–13.

[106] Taiwoo Park, Inseok Hwang, Uichin Lee, Sunghoon Ivan Lee, Chungkuk Yoo, Youngki Lee, Hyukjae Jang, Sungwon Peter Choe, Souneil Park, and Junehwa Song. 2012. ExerLink: enabling pervasive social exergames with heterogeneous exercise devices. In *Proceedings of the 10th international conference on Mobile systems, applications, and services*. 15–28.

[107] Taiwoo Park, Jinwon Lee, Inseok Hwang, Chungkuk Yoo, Lama Nachman, and Junehwa Song. 2011. E-gesture: a collaborative architecture for energy-efficient gesture recognition with hand-worn sensor and mobile devices. In *Proceedings of the 9th ACM Conference on Embedded Networked Sensor Systems*. 260–273.

[108] Taiwoo Park, Uichin Lee, Scott MacKenzie, Miri Moon, Inseok Hwang, and Junehwa Song. 2014. Human factors of speed-based exergame controllers. In *Proceedings of the SIGCHI Conference on Human Factors in Computing Systems*. 1865–1874.

[109] Christine A Pellegrini, Steven D Verba, Amy D Otto, Diane L Helsel, Kelliann K Davis, and John M Jakicic. 2012. The comparison of a technology-based system and an in-person behavioral weight loss intervention. *Obesity* 20, 2 (2012), 356–363.

[110] Igor Pernek, Karin Anna Hummel, and Peter Kokol. 2013. Exercise repetition detection for resistance training based on smartphones. *Personal and ubiquitous computing* 17 (2013), 771–782.

[111] George Pettinico and George R Milne. 2017. Living by the numbers: understanding the "quantification effect". *Journal of Consumer Marketing* 34, 4 (2017), 281–291.

[112] Gerald Pirkl and Paul Lukowicz. 2012. Robust, low cost indoor positioning using magnetic resonant coupling. In *Proceedings of the 2012 ACM Conference on Ubiquitous Computing*. 431–440.

[113] Fazlay Rabbi, Taiwoo Park, Biyi Fang, Mi Zhang, and Youngki Lee. 2018. When virtual reality meets internet of things in the gym: Enabling immersive interactive machine exercises. *Proceedings of the ACM on interactive, mobile, wearable and ubiquitous technologies* 2, 2 (2018), 1–21.

[114] Meera Radhakrishnan, Archan Misra, and Rajesh K Balan. 2021. W8-Scope: Fine-grained, practical monitoring of weight stack-based exercises. *Pervasive and Mobile Computing* (2021), 101418.

[115] Meera Radhakrishnan, Darshana Rathnayake, Ong Koon Han, Inseok Hwang, and Archan Misra. 2020. ERICA: enabling real-time mistake detection & corrective feedback for free-weights exercises. In *Proceedings of the 18th Conference on Embedded Networked Sensor Systems*. 558–571.

[116] Mirana Randriambelonoro, Yu Chen, and Pearl Pu. 2017. Can fitness trackers help diabetic and obese users make and sustain lifestyle changes? *Computer* 50, 3 (2017), 20–29.

[117] Darshana Rathnayake, Meera Radhakrishnan, Inseok Hwang, and Archan Misra. 2023. LILOC: Enabling precise 3D localization in dynamic indoor environments using LiDARs. (2023).

[118] Nirupam Roy, He Wang, and Romit Roy Choudhury. 2014. I am a smartphone and i can tell my user's walking direction. In *Proceedings of the 12th annual international conference on Mobile systems, applications, and services*. 329–342.

[119] Na Jin Seo and Thomas J Armstrong. 2008. Investigation of grip force, normal force, contact area, hand size, and handle size for cylindrical handles. *Human Factors* 50, 5 (2008), 734–744.

[120] Chenguang Shen, Bo-Jhang Ho, and Mani Srivastava. 2017. Milift: Efficient smartwatch-based workout tracking using automatic segmentation. *IEEE Transactions on Mobile Computing* 17, 7 (2017), 1609–1622.

[121] Andrea Soro, Gino Brunner, Simon Tanner, and Roger Wattenhofer. 2019. Recognition and repetition counting for complex physical exercises with deep learning. *Sensors* 19, 3 (2019), 714.

[122] Michael J Stec and Eric S Rawson. 2012. Estimation of resistance exercise energy expenditure using triaxial accelerometry. *The Journal of Strength & Conditioning Research* 26, 5 (2012), 1413–1422.

[123] Mathias Sundholm, Jingyuan Cheng, Bo Zhou, Akash Sethi, and Paul Lukowicz. 2014. Smart-mat: Recognizing and counting gym exercises with low-cost resistive pressure sensing matrix. In *Proceedings of the 2014 ACM international joint conference on pervasive and ubiquitous computing*. 373–382.

[124] Karanbir S Toor, Ameet S Toor, Charlton M Smith, and Alexander G Orozco. 2017. Oli, your weight-training assistant. In *Proceedings of the 2017 CHI Conference Extended Abstracts on Human Factors in Computing Systems*. 184–189.

[125] Eduardo Velloso, Andreas Bulling, Hans Gellersen, Wallace Ugulino, and Hugo Fuks. 2013. Qualitative activity recognition of weight lifting exercises. In *Proceedings of the 4th Augmented Human International Conference*. 116–123.

[126] Fu Xiao, Jing Chen, Xiaohui Xie, Linqing Gui, Lijuan Sun, and Ruchuan Wang. 2018. SEARE: A system for exercise activity recognition and quality evaluation based on green sensing. *IEEE Transactions on Emerging Topics in Computing* 8, 3 (2018), 752–761.

[127] Hongwei Xie, Tao Gu, Xianping Tao, Haibo Ye, and Jian Lv. 2014. MaLoc: A practical magnetic fingerprinting approach to indoor localization using smartphones. In *Proceedings of the 2014 ACM International Joint Conference on Pervasive and Ubiquitous Computing*. 243–253.

[128] Chungkuk Yoo, Inseok Hwang, Seungwoo Kang, Myung-Chul Kim, Seonghoon Kim, Daeyoung Won, Yu Gu, and Junehwa Song. 2017. Card-stunt as a service: Empowering a massively packed crowd for instant collective expressiveness. In *Proceedings of the 15th Annual International Conference on Mobile Systems, Applications, and Services*. 121–135.

[129] Chungkuk Yoo, Inseok Hwang, Eric Rozner, Yu Gu, and Robert F Dickerson. 2016. Symmetrisense: Enabling near-surface interactivity on glossy surfaces using a single commodity smartphone. In *Proceedings of the 2016 CHI Conference on Human Factors in Computing Systems*. 5126–5137.

[130] Chungkuk Yoo, Seungwoo Kang, Inseok Hwang, Chulhong Min, Seonghoon Kim, Wonjung Kim, and Junehwa Song. 2019. Mom, I see You Angry at Me! Designing a Mobile Service for Parent-child Conflicts by In-situ Emotional Empathy. In *Proceedings of the 5th ACM Workshop on Mobile Systems for Computational Social Science*. 21–26.

[131] Aras Yurtman and Billur Barshan. 2014. Automated evaluation of physical therapy exercises using multi-template dynamic time warping on wearable sensor signals. *Computer methods and programs in biomedicine* 117, 2 (2014), 189–207.

[132] Bo Zhou, Mathias Sundholm, Jingyuan Cheng, Heber Cruz, and Paul Lukowicz. 2016. Never skip leg day: A novel wearable approach to monitoring gym leg exercises. In *2016 IEEE International Conference on Pervasive Computing and Communications (PerCom)*. IEEE, 1–9.